Nonequilibrium quantum dissipation in spin-fermion systems

Dvira Segal* and David R. Reichman
Department of Chemistry, Columbia University, 3000 Broadway, New York, New York 10027, USA

Andrew J. Millis
Department of Physics, Columbia University, 538 West 120th Street, New York, New York 10027, USA
(Received 30 August 2007; published 16 November 2007)

Dissipative processes in nonequilibrium many-body systems are fundamentally different than their equilibrium counterparts. Such processes are of great importance for the understanding of relaxation in single-molecule devices. As a detailed case study, we investigate here a generic spin-fermion model, where a two-level system couples to two metallic leads with different chemical potentials. We present results for the spin relaxation rate in the nonadiabatic limit for an arbitrary coupling to the leads using both analytical and exact numerical methods. The nonequilibrium dynamics is reflected by an exponential relaxation at long times and via complex phase shifts, leading in some cases to an "antiorthogonality" effect. In the limit of strong system-lead coupling at zero temperature we demonstrate the onset of a Marcus-like Gaussian decay with *voltage difference* activation. This is analogous to the equilibrium spin-boson model, where at strong coupling and high temperatures, the spin excitation rate manifests temperature activated Gaussian behavior. We find that there is no simple linear relationship between the role of the temperature in the bosonic system and a voltage drop in a nonequilibrium electronic case. The two models also differ by the orthogonality-catastrophe factor existing in a fermionic system, which modifies the resulting line shapes. Implications for current characteristics are discussed. We demonstrate the violation of pairwise Coulomb gas behavior for strong coupling to the leads. The results presented in this paper form the basis of an exact, nonperturbative description of steady-state quantum dissipative systems.

DOI: 10.1103/PhysRevB.76.195316 PACS number(s): 73.63.−b, 03.65.Yz, 05.60.Gg, 72.10.Fk

I. INTRODUCTION

Over the past several decades, tremendous effort has been put forth to understand the dynamics of a small quantum entity coupled to a thermal bath.[1] Important problems that can be distilled to this form include the interaction between localized magnetic impurities and itinerant electrons (the Kondo problem),[2,3] electron transfer in aqueous environments,[4] and proton tunneling in biomolecules.[5,6] The study of such quantum dissipative systems cuts across traditional disciplines and impacts fields from biology to quantum information theory.[1]

Our detailed understanding of quantum dissipative systems is essentially confined to problems which involve a single thermal reservoir.[7] In this case, traditional measures of dynamical interest are equilibrium correlation functions or simple measures of the decay of one-time quantities when the initial condition is not one of thermal equilibrium for the global system. While important for the understanding of various experimental situations, this latter form of nonequilibrium behavior is well understood and generically takes the form of an asymptotic exponential decay to the thermal equilibrium state or the ground state (at zero temperature).[1,7,8]

A less well understood type of nonequilibrium behavior may manifest when a small quantum system is coupled to *more than one reservoir*.[9–22] Here, the generic situation is one of a nonequilibrium steady state, regardless of the initial preparation. Given the fact that this multibath scenario is standard for prospective single-molecule devices[23,24] as well as more general problems, it is imperative to understand the fundamental relaxation motifs that emerge in such nontrivial nonequilibrium cases. Recent work raises the question of whether standard tools borrowed from typical equilibrium quantum dissipative systems are useful in the steady-state nonequilibrium case. For example, the simple equivalence between bosonic and fermionic baths (as obtained via bosonization[25–27]) is lost in the multibath case, while mean-field approaches are fraught with danger due to the fact that a voltage bias may assist tunneling even at zero temperature, rendering the meaning and stability of Hartree-Fock minima unclear.[10,28–31]

While several recent papers have taken up the task of describing the steady state, nonequilibrium dynamics in different model problems, our goal here is a step toward a *detailed and systematic* understanding of dissipative relaxation in the simplest model problems resulting from coupling a small quantum system to several baths, namely, generalized spin-boson models.[9–11] It should be noted that the term "spin-boson" is a misnomer; the interesting and relevant case is that of fermionic reservoirs, which dramatically differ from the case of bosonic reservoirs when the system interacts with more than one bath with different chemical potentials. On the other hand, as in the standard spin-boson model, it is the physics of the x-ray edge singularity[32–35] that forms the fundamental building block of the description of dynamic observables. Here, it is the recently studied nonequilibrium x-ray edge problem[36–42] that lies at the core of the relaxation behavior of standard correlation functions. The more complex physics of the nonequilibrium edge behavior allows for a richer range of dynamical behavior than in the well-studied equilibrium case.

In this paper, we will confine our discussion to calculations that are perturbative in the bare tunneling matrix element of the system but *allow for arbitrarily strong coupling*

to the leads. We will employ both analytical and numerical techniques to describe the dynamics. The numerical approach involves a computational solution of the nonequilibrium x-ray edge problem that is *numerically exact* on all relevant time scales. This will allow us to describe the full crossover behavior from the regime where equilibrium effects dominate to that where the full nonequilibrium behavior (such as bias-induced dephasing and complex phase shifts) is manifested. This is crucial, since the full frequency dependence of relaxation rates and generalized fluctuation-dissipation ratios depend on the entire time history of the dynamics.[11]

We will demonstrate that interesting behavior occurs in specific parameter regimes that lead to antiorthogonality effects and bias-induced tunneling. In particular, the bias-induced tunneling regime at *zero temperature* may display a very broad Gaussian decay of the polarization at strong system-lead coupling. In this regime, the relaxation behavior shows interesting similarities to the usual *high-temperature* Marcus (or semiclassical polaron) behavior,[43–45] with potential bias playing the role of temperature, although crucial differences exist that make these analogies imprecise. Lastly, we investigate the crucial question of the accuracy of the pairwise Coulomb gas decomposition for nonequilibrium steady-state systems. We note that the methods discussed in this work form the basis of a numerically exact path-integral description of quantum dissipation in such nonequilibrium problems.[46]

This paper is organized as follows. In Sec. II, we describe our model system (the out-of-equilibrium spin-fermion model). Section III presents an overview of the analytical results for the nonequilibrium dynamics, along with the relation to the nonequilibrium x-ray edge problem, while Sec. IV presents numerical results. In Sec. V, we present the implications for the tunneling rate. Our results imply a breakdown of the Coulomb gas picture at intermediate times, described in Sec. VI. In Sec. VII, we conclude.

II. MODEL

Our model system consists of a biased two state system (spin) coupled to two electronic reservoirs $n=L,R$ held at different chemical potentials. In what follows, we assume that the temperature is zero and investigate the possibility of *voltage* activated excitation between the spin states. The extension to nonzero temperature is straightforward, both analytically and numerically. The total Hamiltonian is the sum of three terms:

$$H = H_S + H_B^{(f)} + H_{SB}^{(f)}. \tag{1}$$

The spin system H_S consists of a two-level system (TLS) (creation operators $d_\pm^\dagger$) with a bare tunneling amplitude Δ and a level splitting B. The reservoir term $H_B^{(f)}$ includes two noninteracting metallic leads $n=L,R$, where a nonequilibrium state occurs when the leads have different chemical potentials $\Delta\mu=\mu_L-\mu_R\neq 0$. The system-bath interaction $H_{SB}^{(f)}$ couples the spin with scattering processes inside the leads (diagonal coupling) and in between each lead (nondiagonal coupling), and we choose conventions such that only one of the spin levels couples to the leads,

$$H_S = \frac{B}{2}\sigma_z + \frac{\Delta}{2}\sigma_x,$$

$$H_B^{(f)} = \sum_{k,n} \epsilon_k a_{k,n}^\dagger a_{k,n},$$

$$H_{SB}^{(f)} = \sum_{k,k',n,n'} V_{k,n;k',n'} a_{k,n}^\dagger a_{k',n'} n_d(+). \tag{2}$$

Here, $n_d(\pm)=(I\pm\sigma_z)/2$ is the number operator, with I as the identity operator.[47] The operator $a_{k,n}^\dagger$ ($a_{k,n}$) creates (annihilates) an electron with momentum k in the nth lead. In this paper, we focus on the model presented in Ref. 36, where the momentum dependence of the scattering potential is neglected. System-bath scattering potentials are then given by $V_{n,n'}$, where $n,n'=L,R$ are the Fermi sea indices. Our main conclusions, however, are valid for more general cases.

We assume that the reservoirs have the same density of states $\rho(\epsilon)$, typically modeled using a Lorentzian function

$$\rho(\epsilon) = \frac{1}{\pi}\frac{D_L/2}{\left(\frac{D_L}{2}\right)^2 + \epsilon^2}, \tag{3}$$

where D_L is a bandwidth parameter. We typically work in the limit of wide bands, $D_L \gg \Delta\mu$; therefore, to a good approximation, $\rho(\mu_L)\simeq\rho(\mu_R)$.

Note that we ignore the spin degree of freedom of the reservoir electrons in our discussion. In what follows, we refer to the energy difference B as a magnetic field in order to distinguish it from the voltage bias $\Delta\mu$. We also define two auxiliary Hamiltonians $H_\pm$ that will be useful below,

$$H_\pm = \pm\frac{B}{2} + H_{SB}^{(f)}[n_d = \pm] + H_B^{(f)}. \tag{4}$$

Explicitly, $H_\pm$ includes the electronic reservoirs and system-bath interaction, given that the subsystem is in the $\pm$ state.

Model (2) contains much of the physics of the Kondo model[2] while lacking direct coupling of the reservoir degrees of freedom to spin-flip processes. It also contains the spin-resonant-level model of Ref. 11 with a particular choice of system-bath couplings. We discuss the spin-resonant-level model in more detail in Appendix A. The out-of-equilibrium spin-fermion model can be realized in different systems. For example, the relevant effects might be observed within a molecular-based device comprising a molecular chain strongly coupled to the leads with an internal two state system, e.g., different conformations[48] or a spin impurity.[49] Another possible experimental setup is a semiconductor microstructure consisting of two coupled quantum dots, simulating a double-well potential, interacting with a current carrying quantum point contact.[50]

Crucial parameters of the model are the L and R scattering phase shifts. In equilibrium, the phase shifts are given by[32,36]

$$\tan \delta_{\pm} = \frac{1}{2}\{(\alpha_1 + \alpha_2) \pm [(\alpha_1 - \alpha_2)^2 + 4|\nu|^2]^{1/2}\}, \quad (5)$$

where ν and α_n $(n=L,R)$ are dimensionless system-bath coupling strengths,

$$\nu = \pi\rho(\epsilon_F)V_{L,R}, \quad \alpha_1 = \pi\rho(\epsilon_F)V_{L,L}, \quad \alpha_2 = \pi\rho(\epsilon_F)V_{R,R}, \quad (6)$$

and $\rho(\epsilon_F)$ is the density of states at the Fermi energy of the L, R reservoirs. Out of equilibrium, $\Delta\mu \neq 0$, the phase shifts are *complex* numbers given by[36]

$$\tan \delta_L = \alpha_1 + i\frac{|\nu|^2}{1 - i\alpha_2},$$

$$\tan \delta_R = \alpha_2 - i\frac{|\nu|^2}{1 + i\alpha_1}. \quad (7)$$

Since the reservoir density of states weakly varies around the Fermi energy, $D_L \gg \Delta\mu$, the phase shifts are approximately energy independent and are all calculated at the Fermi energy ϵ_F.[36] For simplicity, throughout the paper, we typically consider the case of $\alpha \equiv \alpha_1 = \alpha_2 \ll \nu$ and take $V_{n,n'}$ to be real. We note, however, that our main results, in particular, the appearance of Marcus-type behavior in the nonequilibrium regime at strong coupling, can be rederived using other variants of this model system with no limitations on the strength of the diagonal $V_{n,n}$ interactions, as well as for the spin-resonant-level model of Ref. 11, see Appendix A.

Under these simplifications, the nonequilibrium phase shifts are given by

$$\tan \delta_L = \nu^2(i - \alpha),$$

$$\tan \delta_R = -\nu^2(i + \alpha). \quad (8)$$

For $\alpha=0$, the inverse tangent in Eq. (8) has a branch cut, conventionally placed at $(-i\infty, -i]$ and $[i, i\infty)$. For this special case,

$$\delta_L = -\delta_R = \frac{1}{2}\ln\left(\frac{1+\nu^2}{1-\nu^2}\right). \quad (9)$$

The weak potential limit therefore corresponds to $\delta_+ = -\delta_- \sim \nu$ and $\delta_L = -\delta_R \sim i\nu^2$, so $|\delta_{L,R}| \ll |\delta_{\pm}|$. However, as $\nu \to 1$, $\delta_{L,R}$ diverges, whereas the equilibrium phases $\delta_{\pm}$ are finite.

An important quantity that will be useful below is the sum of the phase shifts squared, $\tilde{\gamma} = -(\delta_L^2 + \delta_R^2)/\pi^2$. While for the general model Eq. (7) yields complex numbers when the system is symmetric $(\alpha_1 = \alpha_2)$, the phase shifts are complex conjugates and $\tilde{\gamma}$ is real, although possibly negative. We discuss the implications of this result in Sec. IV C.

For the sake of completeness and comparison, the *equilibrium* spin-boson model is discussed in Appendix B. In the nonadiabatic limit, this model yields the classical Marcus rate at high temperatures when the system-bath interaction is strong. We analyze the analogous behavior in the nonequilibrium spin-fermion model (2) in Sec. V.

III. NONADIABATIC DYNAMICS

A. Overview

We are interested in the reduced density matrix $\rho_d(t)$ in the space of d occupancy. This is defined in terms of time evolution from an initial condition ρ_i at time $t=0$,

$$\rho_d(t) = \mathrm{Tr}_{leads}[e^{-iHt}\rho_i e^{iHt}]. \quad (10)$$

If the parameter Δ in Eq. (2) vanishes, the problem is just electrons in a time-independent potential, and a closed-form analytical solution exists. If $\Delta \neq 0$, $\rho_d(t)$ may be expressed as an expansion in Δ. Evaluation of any term in the expansion entails solving a problem of electrons in a *time-dependent* field. In equilibrium, an essentially exact closed-form solution exists, and the main problem is to resum the series in Δ.[51,52] For nonequilibrium problems, an analytical expression is not known. In this paper, we present a detailed numerical evaluation of some low order terms in the expansion for Δ. The essential features are revealed by the golden rule decay rate, obtained by assuming that (i) $n_d(+)=0$ at time $t=0$, (ii) ρ_i is the density matrix corresponding to the ground state of H with $n_d(+)=0$, and (iii) that an expansion to $\mathcal{O}(\Delta^2)$ suffices. This level of description is equivalent to the "noninteraction blip approximation" in the standard spin-boson model[1,7,53] and yields the (nonadiabatic) Fermi's golden rule for the forward $(+)$ and backward $(-)$ transition rates between the spin levels as[44,54–56]

$$\Gamma_f^{\pm} = \left(\frac{\Delta}{2}\right)^2 2\,\mathrm{Re}\int_0^{\infty} e^{\pm iBt} C_f(t)dt,$$

$$C_f = e^{iE_- t}\left\langle T\exp\left(-i\int_0^t d\tau H_{SB}^{(f)}(\tau, n_d = +)\right)\right\rangle$$
$$= \langle e^{-iH_+ t} e^{iH_- t}\rangle \equiv e^{-\Phi_f(t)}, \quad (11)$$

where T denotes time ordering, $H_{SB}^{(f)}(t) = e^{iH_B^{(f)}t} H_{SB}^{(f)} e^{-iH_B^{(f)}t}$, and E_- is the ground state energy of the two uncoupled reservoirs. The Hamiltonians $H_{\pm}$ are defined in Eq. (4), Re refers to the real part of the integral, and the trace is performed over the electronic degrees of freedom. For convenience, the term including the energy bias B is taken outside the trace.

The object of our calculation is therefore the correlation function $C_f(t)$, which should be evaluated for nonequilibrium conditions covering time scales from $Dt \sim 1$ up to $\Delta\mu t \gg 1$. D, an energy of the order of the Fermi sea bandwidth, and the potential drop $\Delta\mu$ specify two inverse time scales in the problem, where we typically work in the limit of $\Delta\mu \ll D$. Note that, unlike the equilibrium case, there is no exact analytical approach to calculate $C_f(t)$ valid for all time scales. Approximate analytical approaches and exact numerics may be performed, as discussed below.

B. Short- and long-time asymptotics: Nonequilibrium x-ray edge problem

The correlation function $C_f(t)$ [Eq. (11)] is a crucial element in the theory of the x-ray edge problem, an effect originating from the many-body response of a Fermi system to

the fast switching of a scattering potential, e.g., the creation of a core hole.[32,33] The x-ray edge Hamiltonian is a simplified version of the spin-fermion model, Eq. (2), with a static subsystem that is either empty or populated,

$$H_0 = H_B^{(f)} + \epsilon_d d^\dagger d,$$

$$H_{SB} = \sum_{k,n=L,R} V_{k,n;k',n'} a_{k,n}^\dagger a_{k',n'} d^\dagger d,$$

$$H_{edge} = H_0 + H_{SB}. \tag{12}$$

Here, $d^\dagger$ and d are creation and destruction operators of the core electron, and $a_{k,n}^\dagger$ ($a_{k,n}$) creates (destroys) an electron in the nth lead with momentum k. The *single* band x-ray singularity problem was originally solved exactly in the asymptotic limit by Nozieres–De Dominicis (ND).[32]

In the last ten years, there has been a growing interest in understanding the x-ray edge effect in the mesoscopic regime[34,35] and for nonequilibrium systems,[36–42] where the core hole couples to more than one Fermi sea at different chemical potentials. Standard equilibrium techniques, e.g., bosonization,[25–27] cannot be simply generalized to handle these nonequilibrium systems (see Appendix C). The first to address the nonequilibrium problem was Ng, who generalized the Nozieres–De Dominicis solution to include more than one Fermi sea with different chemical potentials.[36] Ng demonstrated that the edge singularity could be described by generalized phase shifts which are real for equilibrium systems and complex when the system is driven out of equilibrium. Physically, complex phase shifts reflect the finite lifetime of a nonequilibrium system. More recently, Muzykantskii *et al.*[39,40] formally solved the out-of-equilibrium problem using the Riemann-Hilbert approach. The result, given in terms of the scattering matrix, was later generalized to include finite temperature effects.[41] An exact formal determinant solution was presented in Ref. 42 for the study of tunneling in a nonequilibrium electron gas.

A formal solution for $C_f(t)$ is obtained from the linked cluster theorem (valid also for nonequilibrium problems),[32,36]

$$\Phi_f(t) = -\int_0^1 d\lambda \ \mathrm{Tr}\ \underline{\underline{V}}(t)\underline{\underline{G}}^\lambda(t,t), \tag{13}$$

with $\underline{\underline{G}}^\lambda(t,t')$ the matrix Green's function in the space of the leads for Eq. (1), but with $H_{SB} \to \lambda H_{SB}$. For this model, $\underline{\underline{G}}$ solves the Dyson equation

$$\underline{\underline{G}}^\lambda(t_1,t_2) = \underline{\underline{g}}(t_1,t_2) + \int d\tau \underline{\underline{g}}(t_1,\tau)\underline{\underline{V}}^\lambda(\tau)\underline{\underline{G}}^\lambda(\tau,t_2), \tag{14}$$

with $\underline{\underline{V}}^\lambda(\tau) = V_{n,n'} n_d(+)(\tau)$ and the unperturbed Green's functions

$$g_{n,n'}(t_1,t_2) = \frac{\pi\rho}{t_1 - t_2} e^{i(\mu_n t_1 - \mu_{n'} t_2)}. \tag{15}$$

ρ is the reservoir density of states taken to be the same for the L and R leads.

In equilibrium, ND showed[32] that this equation can be solved exactly and the coupling constant integral performed, leading to

$$C_f(t) \sim (Dt)^{-\beta}, \tag{16}$$

with D an energy of the order of the Fermi sea bandwidth, $\beta = (\delta_+^2 + \delta_-^2)/\pi^2$, and $\delta_\pm$ defined in Eq. (5). For the $\alpha = 0$ model studied explicitly,

$$\beta = 2\left(\frac{\arctan(\nu)}{\pi}\right)^2. \tag{17}$$

Equation (16) also holds for the nonequilibrium problem at times $\Delta\mu t \ll 1$.

At long times, $\Delta\mu t \gg 1$, the equation was solved by Ng;[36] see also Ref. 39. The coupling constant integral may similarly be performed, leading to

$$C_f(t) \sim e^{-\Gamma\Delta\mu t}(\Delta\mu t)^\gamma, \tag{18}$$

with $\Gamma = |\delta_L' - \delta_R'|/2\pi$, $\gamma = -(\delta_L^2 + \delta_R^2)/\pi^2$, and $\delta_{L,R}$ given by Eq. (8). Here, δ_n' ($n = L,R$) refers to the imaginary part of the phase shift. For the model studied numerically ($\alpha = 0$), we have

$$\Gamma = \frac{1}{2\pi} \ln\left[\frac{1+\nu^2}{1-\nu^2}\right] \tag{19}$$

and

$$\gamma = \frac{1}{2\pi^2} \ln^2\left[\frac{1+\nu^2}{1-\nu^2}\right]. \tag{20}$$

C. Intermediate time

Although the long-time and short-time behaviors are known essentially exactly, a transparent nonperturbative analytical expression for $C_f(t)$ that encompasses all time scales $\Delta\mu t$ and coupling strengths ρV has not been developed. Indeed, in this work, we argue that at strong coupling ($\nu \to 1$), a different functional form dominates at *intermediate times* $\Delta\mu t \sim 1-10$, where a prominent *Gaussian* decay emerges, $C_f(t) \sim e^{-\kappa(\Delta\mu t)^2}(Dt)^{-\beta}$. We first offer a perturbative calculation which suggests this result and then present exact numerical simulations which prove this behavior. The dominance of the Gaussian behavior at intermediate times translates into a Marcus-type rate in frequency domain, with *bias voltage* activation (see discussion in Sec. V), instead of *temperature* activation, as in the classical Marcus rate (see Appendix B).

The correlation function $C_f(t)$ can be evaluated using the cumulant expansion.[44] Note that unlike the bosonic case, *all* cumulants contribute,

$$C_f(t) = \exp\sum_{n=1}^{\infty} K_n(t),$$

$$K_n(t) = \frac{(-i)^n}{n!}\int_0^t dt_1 \int_0^t dt_2 \cdots \int_0^t dt_n \langle TF(t_1)F(t_2)\cdots F(t_n)\rangle_c, \tag{21}$$

where T denotes time ordering, $F=\Sigma_{k,k',n,n'}V_{n,n'}a^\dagger_{k,n}a_{k',n'}$, and $\langle\cdots\rangle_c$ denotes a cumulant average. The first cumulant yields an energy shift, while the second term is given explicitly by $(Dt>1,\ \alpha=0)$

$$K_2(t) = -\frac{1}{2}\int_0^t dt_1 \int_0^t dt_2 \langle TF(t_1)F(t_2)\rangle_c = -\frac{2\nu^2}{\pi^2}\ln(Dt) - 2\frac{\nu^2}{\pi^2}\Delta\mu t\left[\mathrm{Si}(\Delta\mu t) - \frac{1-\cos(\Delta\mu t)}{\Delta\mu t}\right] + 2\frac{\nu^2}{\pi^2}[\gamma_e + \ln(\Delta\mu t) - \mathrm{Ci}(\Delta\mu t)]. \tag{22}$$

For details, see Appendix D. The sine and cosine integrals are defined as $\mathrm{Si}(x)=\int_0^x \frac{\sin(t)}{t}dt$ and $\mathrm{Ci}(x)=\gamma_e+\ln(x)+\int_0^x \frac{\cos(t)-1}{t}dt$, and $\gamma_e=0.5772$ is the Euler-Mascheroni constant.

This expression reproduces the weak coupling limits of the analytical results, Eqs. (16) and (18) at short and long times, respectively, and provides an interpolation between the two times. In particular, the second term describes how the long-time dissipation $\Gamma\Delta\mu t$ term is "turned on" as $\Delta\mu t$ increases from a small value to values much greater than unity. The first and last terms describe how the equilibrium orthogonality is turned off as $\Delta\mu t$ increases: $[\gamma_e+\ln(\Delta\mu t)-\mathrm{Ci}(\Delta\mu t)-\ln(Dt)]$ is a function which interpolates between $\ln(t)$ for $1/D<t<1/\Delta\mu$ and a constant at $\Delta\mu t\gg 1$. Note that in this model, the leading logarithmic term at long times is $\sim\nu^4$, consistent with the cancellation of logarithmic terms in the long time limit of Eq. (22), i.e., with the absence of a term which "turns on" the nonequilibrium power law. This cancellation does not necessarily occur at order ν^2 in other models, e.g., the spin-resonant-level model, see Appendix A.

We can clearly distinguish between three regimes in Eq. (22):

$$C_f(t) \sim \begin{cases} t^{-2\nu^2/\pi^2} & \Delta\mu t \ll 1 \\ e^{-(\nu\Delta\mu t)^2/2\pi^2} t^{-2\nu^2/\pi^2} & \Delta\mu t \sim 1 \\ e^{-\nu^2\Delta\mu t/\pi} & \Delta\mu t \gg 1. \end{cases} \tag{23}$$

While the first (equilibrium) limit and the third regime are well established in the literature,[11,36,39,40] to the best of our knowledge, the intermediate domain leading to an interesting dynamic has not been discussed before. In the strong coupling limit, the Gaussian behavior may have a dominant effect on the relaxation, as discussed below. We would like therefore to phenomenologically extend the second cumulant expression, Eq. (22), to larger phase shifts (strong coupling).

Perturbative expressions analogous to Eq. (22) motivated Mitra and Millis[10] to propose an interpolation function constructed by replacing the factors of ν^2 in the expression above by the exact phase shifts. For the model considered here, their procedure leads to

$$\Phi_f(t) = +\frac{|\delta_L'' - \delta_R''|}{\pi^2}(\Delta\mu t)\left[\mathrm{Si}(\Delta\mu t) - \frac{1-\cos(\Delta\mu t)}{\Delta\mu t}\right] + \frac{(\delta_+^2+\delta_-^2)}{\pi^2}[\ln(1+iDt) - \gamma_e + \mathrm{Ci}(\Delta\mu t) - \ln(\Delta\mu t)] + \frac{(\delta_L^2+\delta_R^2)}{\pi^2}[\gamma_e - \mathrm{Ci}(\Delta\mu t) + \ln(\Delta\mu t)]. \tag{24}$$

Note that our approximation for the scattering potentials, $\alpha_1=\alpha_2=0$, implies that there is no Fumi energy shift. At the short time limit, $\Delta\mu t\ll 1$, the factor $[\ln(\Delta\mu t)+\gamma_e-\mathrm{Ci}(\Delta\mu t)]$ dies out, leading to the correct equilibrium behavior [Eq. (16)]. In contrast, at long times, the cosine integral diminishes, which implies that the dynamics is ruled by an exponential decay with a rate constant $\Delta\mu\Gamma$ [Eq. (19)] modified by a power-law term t^γ [Eq. (20)].

Our numerical results, to be presented below, show that at weak to moderate coupling, $\nu<0.5$, the correlation function and the resulting transition rates are well described by expression (24). However, Eq. (24) is found to be a poor approximation at strong coupling. Instead, at intermediate times, $\Delta\mu t\sim 1$, we return to Eq. (22) and replace the weak coupling phase shift by the equilibrium strong coupling phase shift, $\nu\to\arctan(\nu)$. The physical picture is that on these time scales, the phase shifts are essentially still the equilibrium ones. Only at longer times $\Delta\mu t\gg 1$ the nonequilibrium dynamics is reflected in the complex phase shifts [Eq. (8)]. This conjecture yields

$$\Phi_f(\Delta\mu t\sim 1) = \Phi_{eq}(t) + \Phi_{neq}(t) + iE_s t, \tag{25}$$

where the equilibrium function is the same as in the zero bias case,[32]

$$\Phi_{eq}(t) = \beta\ln(1+iDt),$$

$$\beta = \frac{(\delta_+^2+\delta_-^2)}{\pi^2} = 2\frac{\arctan^2(\nu)}{\pi^2}, \tag{26}$$

while the nonequilibrium term provides a quadratic time decay,

$$\Phi_{neq}(t) = \kappa(\Delta\mu t)^2,$$

$$\kappa = \frac{(\delta_+^2+\delta_-^2)}{4\pi^2} = \frac{\arctan^2(\nu)}{2\pi^2}. \tag{27}$$

Notice that the prefactor κ depends only on the scattering potential $V_{n,n'}$. The last element in Eq. (25) is the energy shift E_s. We assume that it is given by the equilibrium limit of the Fumi's theorem,

$$E_s = \frac{D}{\pi}[\delta_- + \delta_+]. \tag{28}$$

For $\alpha=0$, the energy shift is zero.

Similar to expressions (25)–(28), Eq. (24) gives the first correction to the equilibrium result which is proportional to $(\Delta\mu t)^2$, but in contrast to these equations, the coefficient involves the nonequilibrium exponent and, in fact, does not provide a wide regime of t^2 behavior. Our numerical simula-

tions, presented below, support expressions (25)–(27) in the broad window $\Delta\mu t \sim 1-10$. We have not been successful in constructing a general analytical expression, valid on all time scales and coupling strengths. It is possible that consideration of the fourth cumulant may yield some insight here.

IV. NUMERICS

A. Methods

The fermionic correlation function $C_f(t)$ can be directly calculated by expressing the zero temperature many-body average as a determinant of the single particle correlation functions,[44,57]

$$C_f(t) = \langle e^{-iH_+t} e^{iH_-t} \rangle = \det[\phi_{k,n;k',n'}(t)]_{k<k_f^n;k'<k_f^{n'}},$$

$$\phi_{k,n;k',n'}(t) = \langle k,n|e^{-ih_+t}e^{ih_-t}|k',n'\rangle. \quad (29)$$

Here, $H_\pm = \Sigma h_\pm$, where $h_\pm$ are the single particle Hamiltonians for the individual conduction electrons. $|k,n\rangle$ are the single particle eigenstates of $H_B^{(f)}$, and the determinant is evaluated over the occupied states. k_f^n is the Fermi energy of the nth reservoir. In our numerical calculations, we have used a Lorentzian density of states, with tails that are long enough to eliminate artificial reflections from the boundaries. The Lorentzian function is centered around the equilibrium Fermi energy with a full width at half maximum D_L, Eq. (3). This quantity sets energy and time scales in our simulations. We have typically used $D_L=4.5$ for the two reservoirs, $\Delta\mu/D_L < 0.1$ and $\nu=0.1-1$. We also take the diagonal coupling to be zero ($\alpha=0$) in all of our simulations, unless otherwise stated. For these parameters, we have found that for short-time evolution ($\Delta\mu t<15$), even for strong coupling, it is satisfactory to model the fermionic reservoirs using ~400 states per bath, where bias is applied by depopulating one of the reservoirs with respect to the other.

We can also employ the renormalization group (RG) method, originally developed by Wilson for the calculation of the thermodynamic properties of the Kondo problem,[58] for the numerical solution of the nonequilibrium x-ray edge problem. In equilibrium, Oliveira and Wilkins[59] and Yoshida *et al.*[60] have used the RG technique to calculate the x-ray absorption spectrum. This study can be generalized to include two reservoirs with different chemical potentials by following a three-step procedure: (i) Define the conduction bands on a logarithmic scale. (ii) Convert the (isolated) reservoir Hamiltonians into semi-infinite tight binding chains, as is done in Refs. 59 and 60. In this representation, the impurity couples the chains' first levels. (iii) Build the Hamiltonians $H_\pm$ in the new basis, first including the occupied levels of the L and R reservoirs and then adding the empty levels. The determinant (29) is performed over occupied levels only.

In equilibrium, the RG technique is highly advantageous over constant and/or Lorentzian discretization methods, as it converges rapidly to the continuum limit even for gross discretization. For small voltage differences ($\Delta\mu/D<10^{-2}$), this method nicely reveals the crossover of $C_f(t)$ from equilibrium to nonequilibrium behavior with increasing bias. In contrast, for large bias, the Lorentzian discretization is more convenient, since energies far from the Fermi energy are not well represented within the RG technique. We present a numerical example in Fig. 1, demonstrating the strength of the RG approach over standard linear discretization for systems in equilibrium. The RG technique provides stable dynamics for long times (full line), where constant discretization fails (dotted line), yielding an artificial rise of the correlation function due to discretization errors. The theoretical value of $\beta=2\arctan^2(\nu)/\pi^2=0.0020$ for $\nu=0.1$ nicely agrees with the numerical slope of 0.0019. Deviations are due to the sharp energy cutoff used at $D_0=1$, with the conduction band energies extending from $-D_0$ to D_0. We also present the results of an RG calculation with a very small voltage drop (dashed line), where linear discretization would require a very fine grid.

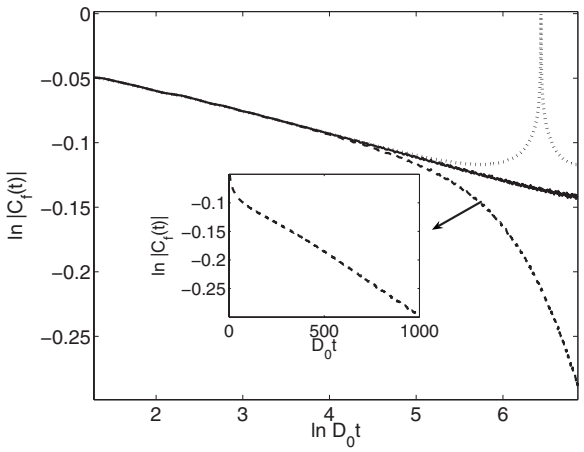

FIG. 1. Decay of $C_f(t)$ as computed by both the RG approach and standard linear discretization for $\nu=0.1$. Constant discretization with 200 states per band, $\Delta\mu=0$ (dotted), showing an artificial rise of the correlation function due to discretization errors; logarithmic discretization (RG) with 100 states per band, $\Lambda=1.1$, $\Delta\mu=0$ (full); logarithmic discretization (RG) with 100 states per band, $\Lambda=1.1$, $\Delta\mu=0.007$ (dashed). Λ is a logarithmic scale parameter, where for each conduction energy there are states with energies ϵ/Λ^m, $m=1,2,\ldots$. Inset: The finite bias case exhibits an exponential decay at long times. The slope agrees with the theoretical value, Eq. (19). The Fermi sea bandwidth is $2D_0$ in all plots with $D_0=1$.

In this work, we typically focus on systems far from equilibrium, $\Delta\mu/D \sim 0.1$. Since the RG method samples the Fermi sea states predominantly near the Fermi energy while high energy states are underrepresented, we find the Lorentzian discretization to be more convenient.

B. Results: $C_f(t)$

Representative results are displayed in Fig. 2. The main plot presents the logarithm of the correlation function $|C_f(t)|$ at strong coupling $\nu=0.95$ for an applied voltage $\Delta\mu=0.24$. Three different regimes are clearly identified: a power-law decay at short times $\Delta\mu t<1$, see lower left inset (a), an exponential decay at long times $\Delta\mu t \gg 1$, and remarkably, an intermediate regime $1 \lesssim \Delta\mu t \lesssim 10$ of approximately Gaussian behavior [upper right inset (b)]. The short- and long-time

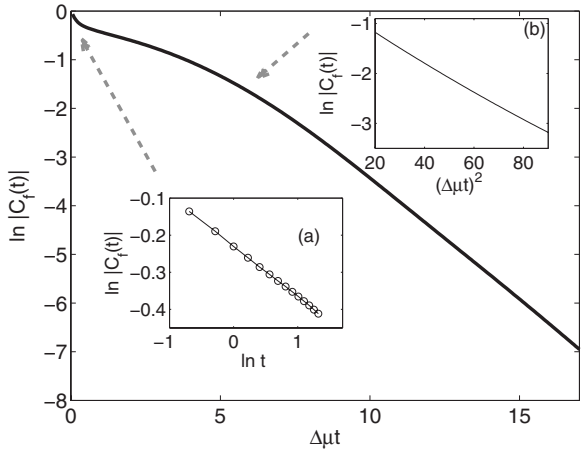

FIG. 2. The correlation function $C_f(t)$ for $\Delta\mu=0.24$, $\nu=0.95$, manifesting (a) a power-law decay at short times $\Delta\mu t<1$ (notice the log-log scale), (b) a Gaussian decay at intermediate times $\Delta\mu t \sim 1-10$, and an exponential decay at long times $\Delta\mu t \gg 1$.

behaviors are consistent with the theoretical results. The intermediate-time quasi-Gaussian regime is an interesting finding with important consequences. We analyze the short-time dynamics $\Delta\mu t<1$, enlarged in Fig. 2(a), by fitting the data to the analytic expression $\ln C_f(t) \sim -\beta \ln(Dt)$. This provides an effective bandwidth $D=6$ and a decay constant $\beta=0.13$ consistent, within numerical errors, with the theoretically expected $\beta=2[\arctan(\nu)/\pi]^2 \approx 0.12$. We can also fit the intermediate-time behavior, shown in Fig. 2(b), by a Gaussian function $\ln C_f(t) \sim -\kappa\Delta\mu^2 t^2$ which yields the prefactor $\kappa=0.03$.

Figure 3 presents a more detailed examination of the Gaussian behavior, showing that at both short and intermediate times, the data can be well described by the approximate function

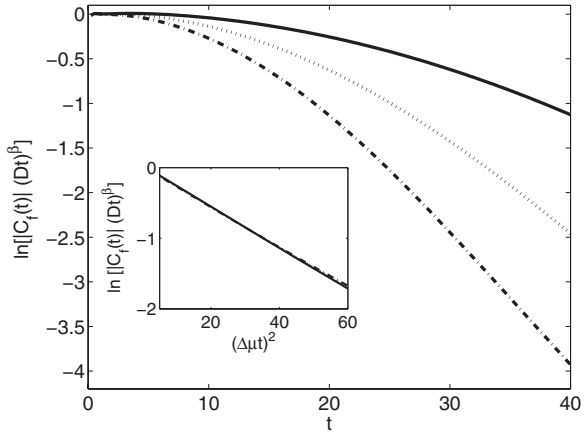

FIG. 3. Evidence for the Gaussian decay at intermediate times $\Delta\mu t \sim 1-10$ and strong coupling $\nu=0.95$, $\Delta\mu=0.16$ (full), $\Delta\mu=0.24$ (dotted), and $\Delta\mu=0.32$ (dashed-dotted). The inset, which includes the three lines one on top of the other, reveals that $C_f(t)t^\beta \propto e^{-\kappa(\Delta\mu t)^2}$, $\beta=0.13$, with $\kappa \sim 0.03$.

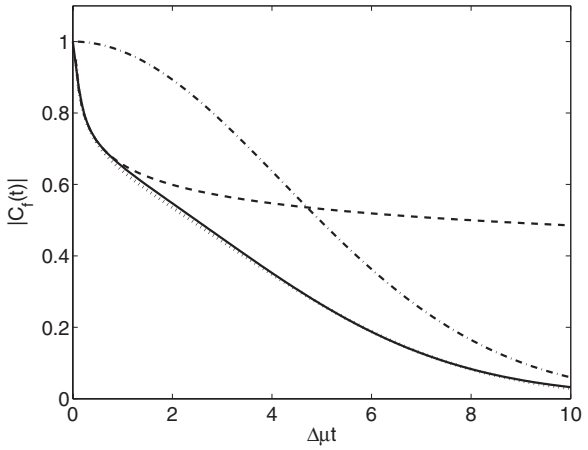

FIG. 4. Time dependence of the correlation function $|C_f(t)|$ for $\Delta\mu=0.24$, $\nu=0.95$. The fitting function $y_G=e^{-\kappa(\Delta\mu t)^2}(Dt)^{-\beta}$ (dotted) with $\kappa=0.03$, $D=6$, and $\beta=0.13$ compared to exact numerical solution (full). The Gaussian (dashed-dotted) and the power-law (dashed) parts of y_G are also displayed separately.

$$y_G(t) = (Dt)^{-\beta} e^{-\kappa(\Delta\mu t)^2}, \tag{30}$$

with β the theoretically predicted short-time (equilibrium) exponent $(\delta_+^2+\delta_-^2)/\pi^2$. The inset proves that the data follow the same linear trend when plotted as a function of $(\Delta\mu t)^2$, with a slope of $\kappa \sim 0.03$. This value nicely agrees with the constant predicted by Eq. (27), $\kappa=\arctan(\nu)^2/2\pi^2=0.029$ $(\nu=0.95)$.

Figure 4 provides more insight by deconstructing the observed time decay of $C_f(t)$ into the equilibrium power-law and nonequilibrium Gaussian components. Another important observation deduced from Figs. 2–4 is that the correlation function decays to ~ 0.1 its initial value by the time the exponential decay begins to dominate. This implies that the Gaussian behavior governs the rate constant at strong enough coupling, leading to a voltage activated regime analogous to the high-temperature semiclassical polaron transport regime. We call this "fermionic Marcus" behavior.

Figure 5 presents the evolution of the correlation function

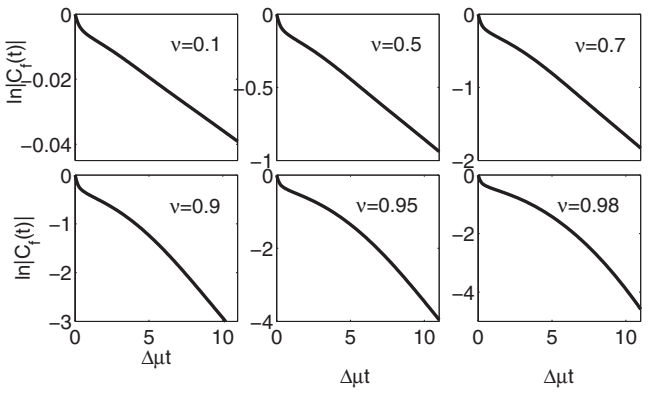

FIG. 5. The correlation function $C_f(t)$ for different coupling strengths ν, manifesting the increasing dominance of intermediate-time Gaussian behavior at strong coupling. $\Delta\mu=0.24$ in all plots.

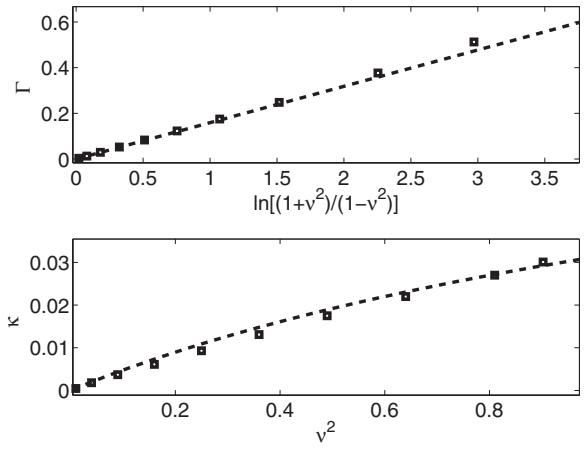

FIG. 6. Testing the validity of Eqs. (19) and (27) for describing the long-time and intermediate-time behaviors, respectively. Top: The relaxation rate Γ. Numerical results calculated from the slope of $\ln[C_f(t)t^\beta]$ vs $\Delta\mu t$ at long times (squares); analytical results using Eq. (19) (dashed line). Bottom: The coefficient κ. The numerical slope of $\ln[C_f(t)t^\beta]$ vs $\Delta\mu^2 t^2$ at intermediate times (squares); analytical results using Eq. (27) (dashed line). These data were computed with $\Delta\mu=0.24$, and β was extracted from the short-time dynamics for each value of ν.

$C_f(t)$ as coupling strength ν is varied from weak to strong. All other parameters are the same as in Fig. 2. For all coupling strengths, the short-time logarithmic and the approximate long-time exponential behaviors are observed. However, as the coupling strength is increased, increasingly wide intermediate regime is observed. We have verified, by an analysis similar to that shown in the lower left inset of Fig. 2, that the short-time behavior is always a power law with the theoretically predicted exponent $\beta=2[\arctan(\nu)/\pi]^2$. Also, note that while at weak coupling ($\nu<0.5$) the correlation function weakly decays before the turnover to an exponential decay takes place, for very strong coupling, $\nu\gtrsim 0.9$, the dynamics is critically controlled by the Gaussian form, as the correlation function has decayed to zero before the exponential decay takes place. This implies that the resulting decay rate [Eq. (11)] essentially shows different characteristics in these two regimes.

We now systematically explore the Gaussian decay at intermediate times and the exponential decay rate at long times and compare the numerical coefficients Γ and κ with the theoretical values, Eqs. (19) and (27), respectively. This is done by calculating the correlation function $C_f(t)$ for coupling strengths $\nu=0.1-0.95$ (see Fig. 5), and then extracting both the quadratic intermediate slope $\kappa\Delta\mu^2$ and the long-time exponential slope $\Gamma\Delta\mu$. Figure 6 presents these coefficients showing excellent agreement with the values predicted from the phenomenological ansatz, Eqs. (25)–(27).

Next, in Fig. 7, we examine the crossover to the analytic long-time behavior, Eq. (24). We compare the numerical correlation function with two functions: the approximate fitting function y_G defined above and the *long-time* perturbation theory result of Ref. 11, given by exponentiating Eq. (24). We refer to this second function as y_E. We see that y_E describes the data well at long times, but that as the coupling

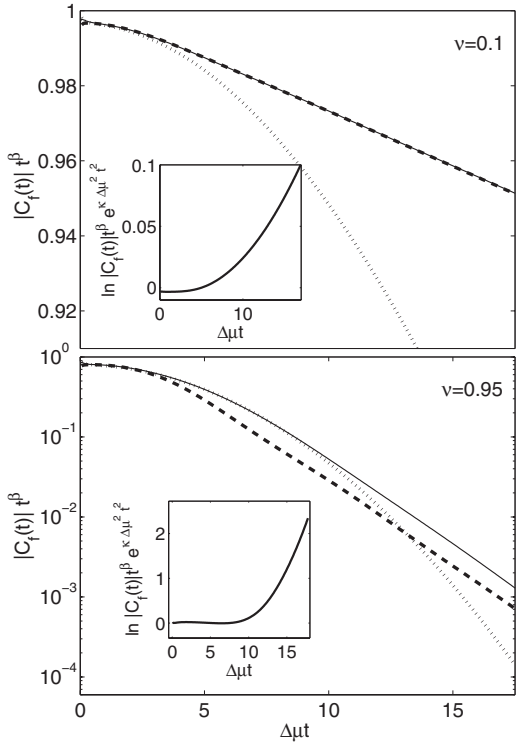

FIG. 7. The turnover from a Gaussian decay to an exponential relaxation. Top: Comparison between the numerical correlation function $C_f(t)$ (full) and the fitting functions y_G (dotted) and y_E (dashed) defined in the text, $\nu=0.1$, $\Delta\mu=0.24$. Inset: Exposing the turnover by taking away the short-time and intermediate-time terms $t^{-\beta}e^{-\kappa\Delta\mu^2t^2}$ with $\beta=0.002$, $\kappa=5\times10^{-4}$. Bottom: Same with $\nu=0.95$, leading to $\beta=0.13$, $\kappa=0.03$. While y_G explicitly includes the Gaussian decay, correct to $\Delta\mu t\sim 10$, the function y_E captures the correct slope at longer times.

strength is increased, the range over which the Gaussian description applies increases. This feature can be qualitatively described by the approximate crossover function

$$C_f^{(app)}(t)\sim\exp\left\{-\left[(\Gamma\Delta\mu t)^2+\frac{\Gamma^4}{4\kappa^2}\right]^{1/2}+\frac{\Gamma^2}{2\kappa}\right\}, \quad (31)$$

which captures the crossover from a Gaussian dynamics to an exponential decay. An increase of ν leads to a strong enhancement of Γ, while κ reaches saturation, resulting in a counterintuitive lengthening of the range of the intermediate Gaussian dynamics with increased Γ.

In summary, we have shown that the crossover between equilibrium ($\Delta\mu t\ll 1$) and nonequilibrium ($\Delta\mu t\gg 1$) behaviors is described by a regime of Gaussian relaxation negligible for weak coupling, but for strong coupling extending over the wide range $1\lesssim\Delta\mu\lesssim 10$, with parameters determined by the equilibrium exponents. In Sec. V, we examine the consequences for spin relaxation.

C. Orthogonality and antiorthogonality

We focus next on the power-law contribution to Eq. (18). Unlike the standard equilibrium case, where the system al-

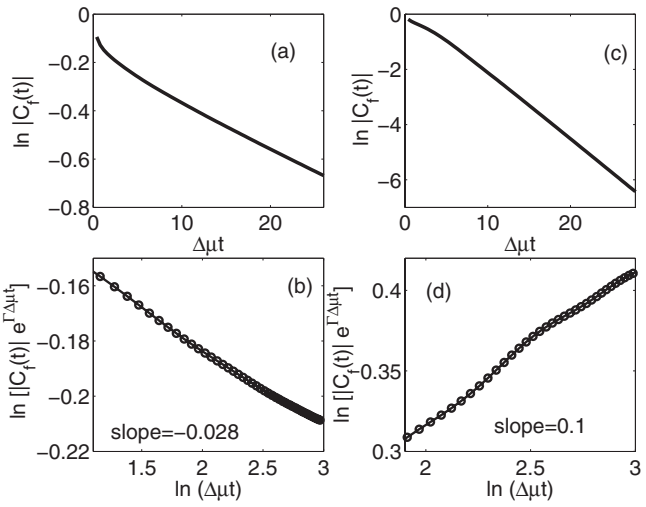

FIG. 8. Orthogonality and antiorthogonality effects in the nonequilibrium system $\Delta\mu=0.4$. [(a) and (b)] $\nu=0.3$, $\alpha=0.5$, manifesting the standard orthogonality effect ($\tilde{\gamma}<0$). [(c) and (d)] $\nu=0.8$, $\alpha=0$, revealing the antiorthogonality effect ($\tilde{\gamma}>0$).

ways experiences dephasing, $\gamma<0$,[61] in our model, the power-law term in Eq. (18) acquires a positive exponent $\gamma>0$, *enhancing* the correlation function, see Eq. (20). We refer to this situation as an "antiorthogonality" effect. For a general system-bath coupling model, Eq. (24) reveals that

$$C_f(\Delta\mu t \gg 1) \sim e^{-\Gamma\Delta\mu t}t^{\tilde{\gamma}}, \quad \tilde{\gamma}=-(\delta_L^2+\delta_R^2)/\pi^2, \qquad (32)$$

with complex, nonequilibrium phase shifts given by Eq. (7).[36] It is clear that in the special limit of zero diagonal interactions ($\alpha=0$), the phase shifts $\delta_{L,R}$ are purely imaginary and $(\delta_L^2+\delta_R^2)<0$ for all values of ν, leading to $\tilde{\gamma}>0$. In contrast, for large diagonal coupling, we typically find that $\tilde{\gamma}<0$, which is the standard orthogonality behavior. The antiorthogonality effect is therefore *a footprint* of a nonequilibrium situation.

We next turn to a numerically exact exploration of the antiorthogonality effect. Figure 8 shows the correlation function $C_f(t)$ at long times $\Delta\mu t \gg 1$ when expression (24) holds. We numerically extract the long-time slope $\Gamma\Delta\mu$ and recover the weak power-law dependence by multiplying the correlation function by the inverse of the exponential decay. The standard orthogonality effect is presented in panels (a) and (b) for $\alpha=0.5$ and $\nu=0.3$, for which $\tilde{\gamma}=-0.038$. When $\alpha=0$ and $\nu=0.8$, the antiorthogonality effect clearly manifests itself with $\tilde{\gamma}=0.12$ [(c) and (d)]. Interestingly, the correlation function at long times shows a complicated behavior, more complex than that predicted in Eq. (24), as evidenced by the mild deviations from strict power-law behavior displayed in Fig. 8(d).

Figure 9 presents an "orthogonality-antiorthogonality" map as a function of the diagonal (α) and nondiagonal (ν) couplings using the general expressions of Eq. (7) with $\alpha=\alpha_1=\alpha_2$. We find that for large α, $-1/2<\tilde{\gamma}<0$, manifesting the standard orthogonality effect. For large nondiagonal interactions, typically antiorthogonality may be observed.

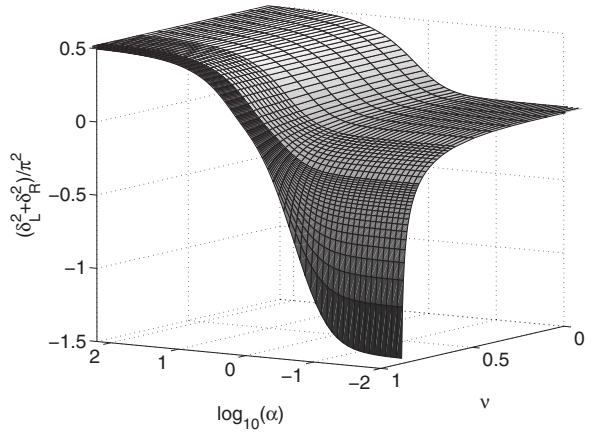

FIG. 9. Map of orthogonality $[(\delta_L^2+\delta_R^2)>0]$ and antiorthogonality $[(\delta_L^2+\delta_R^2)<0]$ behaviors using expression (7) with $\alpha=\alpha_1=\alpha_2$.

In addition to the long-time exponential decay and antiorthogonality behavior, nonequilibrium dynamics may be reflected in the appearance of complex power-law exponents.[36] When the spin impurity is symmetrically coupled to the two leads ($\alpha_1=\alpha_2$), the phase shifts are complex conjugates, see Eq. (7), and $\tilde{\gamma}$ is always real. This situation was discussed above. In contrast, *asymmetric* systems may acquire a complex coefficient with $\tilde{\gamma}=\tilde{\gamma}+i\tilde{\gamma}'$, a direct outcome of a nonequilibrium situation.

The imaginary contribution to $\tilde{\gamma}$ is resolved in Fig. 10. Since at weak coupling the imaginary term $\tilde{\gamma}'$ is very small, we investigate a strong coupling system with $\nu=0.95$. Motivated by Eq. (24), we assume the generic form $C_f(t)=|C_f(t)|e^{i\epsilon t}e^{i\tilde{\gamma}'\ln t}$. We numerically extract the phase factor ϵ, and then plot the function $I(t)=C_f(t)/|C_f(t)|e^{-i\epsilon t}$ for different diagonal coupling strengths. As expected, in symmetric situations, $I(t)\sim 1$. In contrast, asymmetric systems $(\alpha_1\neq\alpha_2)$ reveal an additional decaying contribution which is expected to oscillate at longer times. We did not succeed in fitting $I(t)$ to the stretched-oscillatory function $e^{i\tilde{\gamma}'\ln t}$, indicating that at strong coupling, the dynamics is more involved. Finally, we

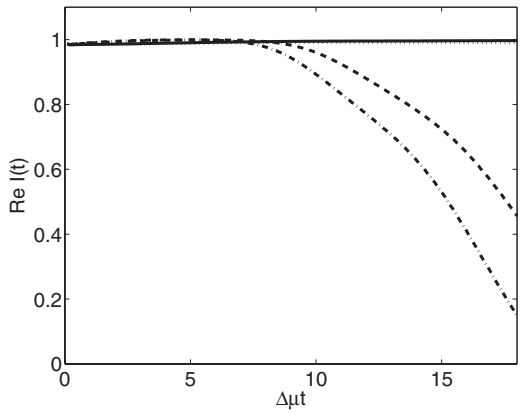

FIG. 10. Resolving the complex part of the power-law exponent $\tilde{\gamma}$. $\alpha_1=0$, $\alpha_2=0$ (full); $\alpha_1=0.1$, $\alpha_2=0$ (dashed); $\alpha_1=0.2$, $\alpha_2=0$ (dashed-dotted); $\alpha_1=0.2$, $\alpha_2=0.2$ (dotted); $\Delta\mu=0.24$ and $\nu=0.95$ in all plots.

note that, consistent with our observations above, equilibrium effects dominate up to $\Delta\mu t \sim 10$. Only at longer times $I(t)$ begins to deviate from unity due to the emerging influence of the imaginary term $\tilde{\gamma}'$.

Though the imaginary term $\tilde{\gamma}''$ can strongly affect the correlation function $C_f(t)$, (Fig. 10), its practical contribution to the golden rule rate is small. We find that for weak to intermediate coupling, $\tilde{\gamma} \ll 1$, leading to $I(t) \sim 1$. On the other hand, for strong coupling, $\tilde{\gamma}''$ manifests itself only at long times, $\Delta\mu t > 10$, when the correlation function has essentially decayed to zero.

V. RELAXATION

A. Qualitative discussion

In this section, we present calculations of the nonadiabatic relaxation rates $\Gamma_f^{\pm}(\omega)$ defined in Eq. (11). The given physical model corresponds to two states separated by an energy ω which depends on the bare level splitting B and on renormalizations arising from the coupling to the leads. $\Gamma_f^+(\omega < 0)$ corresponds to the up-scattering rate describing transitions from the lower level to the upper level, while $\Gamma_f^+(\omega > 0)$ corresponds to down-scattering. In equilibrium at $T=0$, $\Gamma_f^+(\omega < 0) = 0$, i.e., there is no up-scattering. At temperature $T > 0$, the detailed balance relation of equilibrium thermodynamics implies $\Gamma_f^+(-\omega)/\Gamma_f^+(\omega) = e^{-\omega/T}$. In this section, we examine the rates in the nonequilibrium situation. We show that the Gaussian form of the correlation function $C_f(t)$ which occurs at strong coupling has important consequences for the physics.

Before discussing our results in detail, we establish the relevant energy scales. The general expression, Eq. (11), may be written (neglecting overall factors) as

$$\Gamma_f^+(\omega) = \mathrm{Re} \int_0^\infty \frac{dt}{(iDt)^{\beta_{eff}(t)}} e^{i\omega t - A(t)}. \tag{33}$$

Here, $\beta_{eff}(t)$ is an effective exponent which changes from the equilibrium power β, Eq. (17), to the nonequilibrium value β_{neq} [defined as $(-\gamma)$ in Eq. (20)], as $\Delta\mu t$ changes from less than unity to much great then unity. ω is the physical energy level difference, given by the sum of B [Eq. (2)] and the level shift arising from the system-bath coupling, and D is an energy scale of the order of the Fermi sea bandwidth.

The naive assumption[10] is that the only important energy scale is the relaxation rate given by the current flow across the system, $\Gamma\Delta\mu$. In fact, the numerical and analytical results presented in the previous sections indicate that the situation is more subtle. At short times, $A(t) \approx \kappa(\Delta\mu t)^2$, whereas at long times, $A(t) \to \Gamma\Delta\mu t$. The interplay of κ, which is proportional to coupling strength ν^2 at weak coupling but saturates at strong coupling [Eq. (27)], and Γ, which is proportional to ν^2 at weak coupling but diverges at strong coupling [Eq. (19)], gives a richer behavior.

Appendix E gives details of an asymptotic analysis of Eq. (33). This analysis reveals that to discuss the relaxation rate, one should distinguish strong and weak couplings. In the weak coupling limit, there are two relevant scales, $\Gamma\Delta\mu$ and $\Delta\mu$ (the latter multiplied by various factors which are in practice fairly close to unity). For $\omega > \Delta\mu$, we get the equilibrium down-scattering rate; for $|\omega| < \Delta\mu$, we find a nontrivial approximately Lorentzian behavior, and for $\omega < -\Delta\mu$, we reproduce the $e^{-(\omega/\Delta\mu)\ln(\omega/\Delta\mu)}$ behavior found by Mitra *et al.*[10] Specifically,

$$\Gamma_f^+(\omega) = \tilde{\Gamma}(1-\beta)\frac{\sin(\pi\beta)}{\omega}\left(\frac{\omega}{D}\right)^\beta, \quad \omega > \Delta\mu,$$

$$\Gamma_f^+(\omega) = \frac{\Gamma\Delta\mu}{\omega^2 + \Gamma^2\Delta\mu^2}, \quad -\frac{\Delta\mu}{\ln\Gamma} < \omega < \Delta\mu,$$

$$\Gamma_f^+(\omega) \sim e^{-(\omega/\Delta\mu)\ln(\omega/\Delta\mu)}, \quad \omega < -\frac{\Delta\mu}{\ln\Gamma}. \tag{34}$$

Here, $\tilde{\Gamma}(x)$ is the complete gamma function. Note that the formulas match at $\omega \simeq \Delta\mu$ because in weak coupling, $\beta \simeq \Gamma \ll 1$ leading to $\Gamma_f^+(\omega \sim \Delta\mu) \propto 1/\omega$. In the strong coupling limit, two frequency scales turn out to be important: $\sqrt{\kappa}\Delta\mu$ and $\Gamma\Delta\mu$. We find

$$\Gamma_f^+(\omega) = \tilde{\Gamma}(1-\beta)\frac{\sin(\pi\beta)}{\omega}\left(\frac{\omega}{D}\right)^\beta, \quad \omega \gtrsim \sqrt{\kappa}\Delta\mu, \tag{35}$$

$$\Gamma_f^+(\omega) = e^{-[\omega^2/4\kappa(\Delta\mu)^2]}\frac{\tilde{\Gamma}[(1-\beta)/2]\cos\dfrac{\pi\beta}{2}}{2\sqrt{\kappa}\Delta\mu}\left(\frac{\sqrt{\kappa}\Delta\mu}{D}\right)^\beta, \quad |\omega| \lesssim \sqrt{\kappa}\Delta\mu, \tag{36}$$

$$\Gamma_f^+(\omega) = e^{-[\omega^2/4\kappa(\Delta\mu)^2]}\frac{\cos(\pi\beta)}{2\sqrt{\kappa}\Delta\mu}\left(\frac{2\kappa\Delta\mu^2}{D\omega}\right)^\beta, \quad -\Gamma\Delta\mu \lesssim \omega \lesssim -\sqrt{\kappa}\Delta\mu, \tag{37}$$

$$\Gamma_f^+(\omega) \sim e^{-(\omega/\Delta\mu)\ln(\omega/\Delta\mu)}, \quad \omega < -\Gamma\Delta\mu. \tag{38}$$

The Gaussian behavior found at intermediate frequency scales is a consequence of the wide regime of t^2 behavior found in the time evolution function and may be roughly understood as the Fourier transform of $e^{-\kappa(\Delta\mu t)^2}$, although as the results of Appendix E show, this argument must be treated with some care.

We call Eqs. (36) and (37) the "fermionic Marcus rate," the analog of the classical Marcus result for spin-boson systems [Eq. (B12)], which holds in nonequilibrium situations at strong coupling. This expression indicates that the voltage *activates* the absorption rate, similarly to the role of temperature in the bosonic case. The result differs from the bosonic solution (Appendix B) in some important aspects: (i) In the fermionic case, the Gaussian decay is modified by a weak power law term. (ii) For bosonic systems, the activation factor depends on the temperature as $\ln\Gamma_f \propto T^{-1}$, while for fermionic systems, we get a voltage squared activation, $\ln\Gamma_f \propto \Delta\mu^{-2}$. Therefore, there is no simple linear mapping between temperature and voltage drop in the strong coupling regime. We note, however, that the classical Marcus rate is

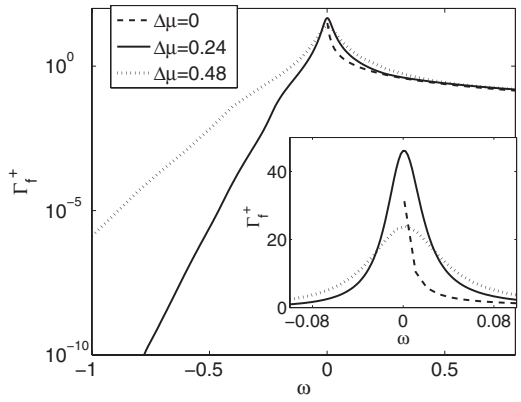

FIG. 11. Golden rule relaxation rate calculated for the weak coupling limit $\nu=0.5$ ($\beta=0.043$, $\Gamma=0.08$); $\Delta\mu=0$ (dashed line), $\Delta\mu=0.24$ (solid line), and $\Delta\mu=0.48$ (dotted line). The inset presents an expanded view of low frequency regime.

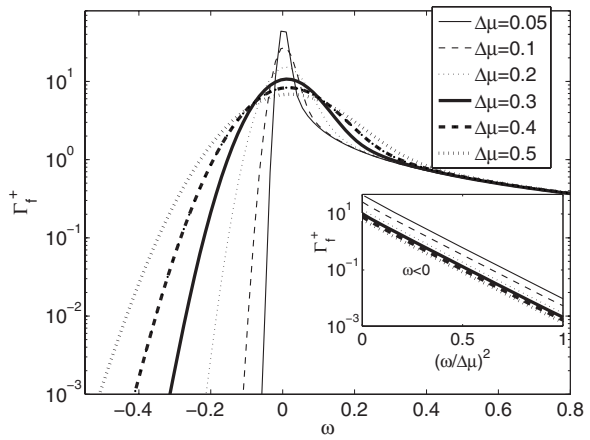

FIG. 12. Fermi's golden rule rate, Eq. (33), as a function of frequency. $\kappa=0.03$ and $\beta=0.13$ ($\nu=0.95$). Inset: Voltage activated excitation rate ($\omega<0$).

applicable in the high temperature limit (see Appendix B), while we typically assume here that $\Delta\mu \ll D$. Therefore, in our system, the energy window for reorganization processes is the bias voltage, rather than the full bandwidth D. Thus, we may interpret the $\kappa\Delta\mu^2$ factor in the denominator of the Gaussian decay [Eq. (37)] as a reorganization energy of the nonequilibrium fermionic system, $\lambda_f \sim \kappa\Delta\mu$, multiplied by the driving force $F_f \equiv \Delta\mu$. In contrast, in the equilibrium spin-boson model, reorganization energies are of order of the cutoff frequency, $\lambda_b \propto \omega_c$, and the driving force for absorption processes is temperature $F_b \equiv T$. Qualitatively, both models then recast to the familiar Marcus-like form, $\Gamma \propto e^{-\omega^2/\lambda F}$.[62] Further, both the fermionic and the standard Marcus behaviors share similar qualitative features such as the existence of an inverted regime, as discussed in the next section.

B. Numerics: Rates, population, and current

We numerically evaluate integral (33) using the coefficients Γ, γ, β, and κ as determined by the coupling strengths, Eqs. (19), (20), (26), and (27), respectively. For convenience, we disregard the multiplicative factor $\Delta^2/2$.

The main panel of Fig. 11 shows on a semilogarithmic scale the relaxation rate computed numerically for the relatively weak coupling $\nu=0.5$ ($\beta=0.043$, $\Gamma=0.08$, and nonequilibrium exponent $\beta_{neq}=-\gamma=0.013$) and two choices of chemical potential, $\Delta\mu=0.24$ and $\Delta\mu=0.48$. Also shown as the dashed line is the $T=0$ equilibrium result. The inset shows an expanded view of the small frequency regime, demonstrating the Lorentzian behavior. We clearly observe the three regimes as discussed in Eq. (34): For small frequencies (large bias voltage), the spin levels are approximately degenerate, and the rates are symmetric around $\omega=0$ (inset). In the opposite $|\omega|>\Delta\mu$ limit, the absorption rate is practically zero, while the emission rate approaches the equilibrium limit. In between, a voltage activated excitation behavior is revealed.

We analyze next the strong coupling limit. Figure 12 shows that the excitation process is activated by a finite potential difference as prescribed by Eq. (37). More quantitatively, the inset verifies that the relationship $\ln \Gamma_f^+(\omega<0) \propto -(\omega^2/\Delta\mu^2)$ holds. Similar to classical bosonic Marcus rate,[45] an inverted regime appears for the fermionic system. However, in the present case, the rate in the inverted regime decays *weakly* as a power law rather than as a Gaussian. At large frequencies, $\omega \gg \Delta\mu$, equilibrium behavior is observed where $\Gamma_f^+(\omega<0)$ approached zero and $\Gamma_f^+(\omega>0)$ becomes insensitive to voltage. We have also calculated the golden rule rate using the *numerical* correlation function (depicted, e.g., in Figs. 2 and 3), instead of the approximate analytical function in Eq. (33), and find that the results agree perfectly.

We now turn to a study of the spin polarization. In the incoherent tunneling regime, for small tunneling parameter Δ, the populations of the two levels obey a Markovian balance equation

$$\dot{P}_+ = \Gamma_f^- P_- - \Gamma_f^+ P_+, \quad P_- + P_+ = 1, \tag{39}$$

with the absorption and emission rates given by Eq. (33). The polarization $\langle\sigma_z\rangle \equiv P_+ - P_- = \frac{\Gamma_f^- - \Gamma_f^+}{\Gamma_f^+ + \Gamma_f^-}$, shown in Fig. 13, manifests a transition from a fully polarized system $\langle\sigma_z\rangle \sim -1$ to an unpolarized system $\langle\sigma_z\rangle \sim 0$ as $\Delta\mu$ is increased. Typically, we find that the crossover takes place when the energy bias ω becomes comparable to the bias voltage. While at high frequencies, $|\omega| \gg \Delta\mu$, $\Gamma_f^+(\omega<0) \sim 0$, leading to full polarization, at very large bias, the emission and absorption rates are comparable, resulting in equal populations of the two levels and zero polarization. The Gaussian activation term in Eq. (37) is therefore reflected in the enhancement of polarization with bias voltage.

It is also interesting to note that the electron current through the system, calculated at the level of mean-field theory, $I \propto \Delta\mu \langle n_d(+)\rangle^2$, is strongly suppressed for weak bias, $\Delta\mu < \omega$, see inset of Fig. 13. In contrast, for very large bias, $\langle n_d(+)\rangle = 1/2$, and the current increases linearly with $\Delta\mu$. Therefore, it is the intermediate regime of $\omega \sim \Delta\mu$ that manifests prominent nonlinear current-voltage characteristics, emerging due to the interplay between the Gaussian relax-

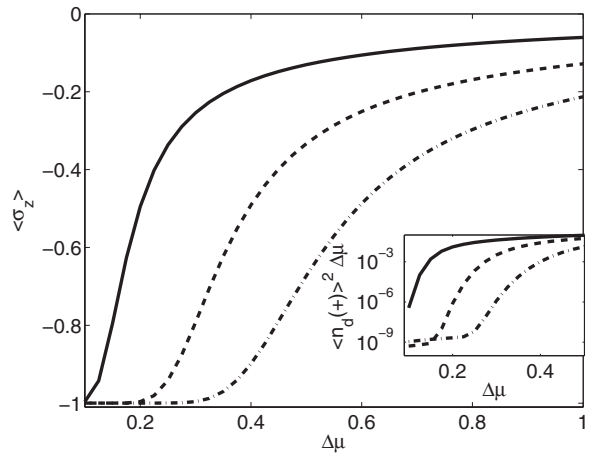

FIG. 13. Spin polarization as a function of potential bias $\Delta\mu$ for different energy biases $\omega=0.1$ (full), $\omega=0.2$ (dashed), and $\omega=0.3$ (dashed-dotted) for $\kappa=0.03$, $\beta=0.13$ ($\nu=0.95$). Inset: Mean-field calculation of the current $I\propto\langle n_d(+)\rangle^2\Delta\mu$ for the same frequencies as in the main plot.

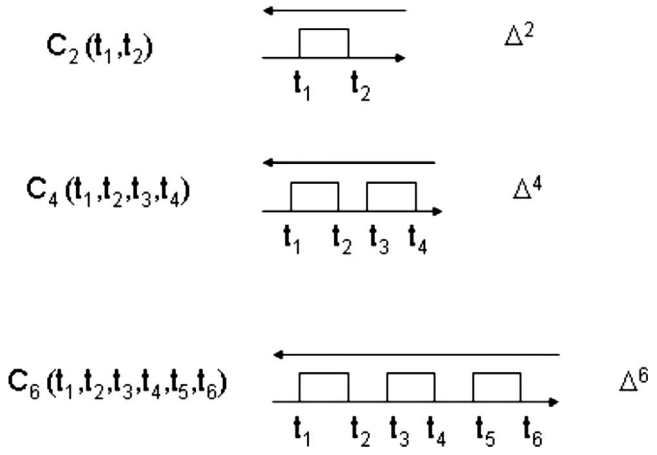

FIG. 14. Schematic representation of spin-flip events on the Keldysh contour. Plotted are examples for particular two, four, and six spin-flip processes, respectively.

ation and the power-law dynamics. We can compare our results to the weak coupling Bloch-type rate equations of Gurvitz[63] which yield $\langle\sigma_z\rangle=0$ at long enough times, independent of voltage drop and energy bias. In contrast, Fig. 13 reveals a rich dynamics in the strong coupling regime with a prominent dependence on system energetics and the nonequilibrium conditions.

VI. BEYOND $\mathcal{O}(\Delta^2)$: COULOMB GAS BEHAVIOR

In this section, we discuss a crucial ingredient of the physics of our model that allows for a description beyond the golden rule $[\mathcal{O}(\Delta^2)]$ level. A formally exact solution for the impurity spin problem (2) can be written by a power series in the tunneling matrix element Δ.[64] Here, we restrict ourselves to an exact numerical investigation of the electronic correlation functions that appear in this power series to see if the usual "Coulomb gas" behavior is observed even when the system is out of equilibrium. In particular, the reduced density matrix of the spin impurity $\rho_d(t)$ is given by

$$\rho_d(t)=\mathrm{Tr}[e^{-iHt}\rho(0)e^{iHt}], \tag{40}$$

with forward and backward time evolution branches. Here, ρ is the total density matrix, and the trace is performed over the reservoir electronic states. We decompose the propagators, including all spin-flip events along the time ordered contour, and obtain, e.g., for the spin up population,[7,64]

$$\langle+|\rho_d(t)|+\rangle=\sum_{k=0}^{\infty}\sum_{j=0}^{\infty}(-1)^{(k+j)}\left(\frac{\Delta}{2}\right)^{2k+2j}\int_0^t dt_1\cdots\int_0^{t_{2k-1}}dt_{2k}\int_0^t ds_1\cdots\int_0^{s_{2j-1}}ds_{2j}\,\mathrm{Tr}[(e^{iH_+s_{2j}}e^{-iH_-s_{2j}})\cdots(e^{iH_-s_1}e^{-iH_+s_1})$$
$$\times(e^{iH+t_1}e^{-iH_-t_1})\cdots(e^{iH_-t_{2k}}e^{-iH_+t_{2k}})]. \tag{41}$$

Here, $|\pm\rangle$ are the up and down spin states, and $H_\pm$ is defined in Eq. (4). This expression was derived assuming that at $t=0$, the spin is in the pure state $|+\rangle$, and the (isolated) reservoirs are in their respective ground states ($T=0$). It can be easily generalized to describe other initial conditions. Each time variable in Eq. (41) marks a particular spin-flip event. While the second order correlation function couples nearest neighbor events only, higher order correlations couple distant spin flips, yielding a multiparticle interaction term. In equilibrium, this interaction can be exactly written in terms of pairwise contributions, $\mathrm{Tr}[\cdots]\propto\exp[\Sigma_{k<j}(-1)^{k+j}\Phi_f(t_k-t_j)]$, significantly simplifying the computational problem. This is the celebrated Anderson-Yuval-Hamann (AYH) result, which leads to the interpretation of the Kondo problem as a one-dimensional Coulomb gas system.[65] In contrast, in the general nonequilibrium case, the exact structure of the interaction is not known for all times, and it is not clear whether higher order correlations can be exactly decomposed into pairwise contributions.[13]

Using the numerical technique discusses in Sec. IV, we can exactly calculate, term by term, the correlation functions in Eq. (41). Specifically, we study three examples of the processes of the order of Δ^2, Δ^4, and Δ^6, depicted schematically in Fig. 14,

$$C_2(t_1,t_2) = \langle e^{iH_-t_1} e^{iH_+(t_2-t_1)} e^{iH_-(t-t_2)} e^{-iH_-t} \rangle$$

$$C_4(t_1,t_2,t_3,t_4) = \langle e^{iH_-t_1} e^{iH_+(t_2-t_1)} e^{iH_-(t_3-t_2)} e^{iH_+(t_4-t_3)} e^{iH_-(t-t_4)} e^{-iH_-t} \rangle$$

$$C_6(t_1,t_2,t_3,t_4,t_5,t_6) = \langle e^{iH_-t_1} e^{iH_+(t_2-t_1)} e^{iH_-(t_3-t_2)} e^{iH_+(t_4-t_3)} e^{iH_-(t_5-t_4)} e^{iH_+(t_6-t_5)} e^{iH_-(t-t_6)} e^{-iH_-t} \rangle, \tag{42}$$

and compare the results to the Coulomb gas expressions

$$\tilde{C}_2(t_1,t_2) \equiv C_2(t_1,t_2) = C_2(t_2-t_1),$$

$$\tilde{C}_4(t_1,\ldots,t_4) = \frac{C_2(t_2-t_1)C_2(t_4-t_1)C_2(t_3-t_2)C_2(t_4-t_3)}{C_2(t_3-t_1)C_2(t_4-t_2)},$$

$$\tilde{C}_6(t_1,\ldots,t_6) = \tilde{C}_4(t_1,\ldots,t_4)\frac{C_2(t_6-t_1)C_2(t_5-t_2)C_2(t_6-t_3)C_2(t_5-t_4)C_2(t_6-t_5)}{C_2(t_5-t_1)C_2(t_6-t_2)C_2(t_5-t_3)C_2(t_6-t_4)}. \tag{43}$$

In particular, our calculations were performed assuming a regular interval τ between spin flips.

We have robustly checked that the AYH decomposition[65] holds precisely at all times (greater than $D\tau > 1$) and coupling strengths in equilibrium, as well as for all times out of equilibrium, for weak to intermediate coupling strengths, see Figs. 15 and 16. Interestingly, the AYH decomposition breaks down for the strong coupling out-of-equilibrium situation, precisely in the time window where $C_f(t)$ shows a broad Gaussian decay with time, as depicted in Fig. 5. Even in this regime, the pairwise AYH decomposition holds asymptotically for long and short times.

An important outcome of this observation is that the AYH Coulomb gas expression,[65] which is exact in equilibrium, cannot be justified for intermediate times $\Delta\mu \sim 1-10$ for strong coupling to the leads in the out-of-equilibrium situation. This is because at strong coupling, the effective short-time behavior (which cannot be described by the Coulomb gas picture) practically extends to longer times of order $\Delta\mu t \sim 1-10$. The Coulomb gas expression still holds for weak to intermediate coupling strength and at long times. This investigation lays the groundwork for an exact evaluation of the spin dynamics via path-integral techniques valid even when the Coulomb gas decomposition does not hold. This work will be reported in a future publication.[46]

VII. SUMMARY

In this paper, we have undertaken a detailed study of the nonequilibrium dynamics of a small quantum system coupled to two electronic leads. This problem is of great interest for understanding dissipative effects in prospective single-molecules devices. The model studied here is generic enough to capture range of relevant relaxation motifs while being simple enough for detailed investigation. Our analysis combines analytical results with exact numerics, rendering a detailed and clear picture of the dissipative behavior on *all*

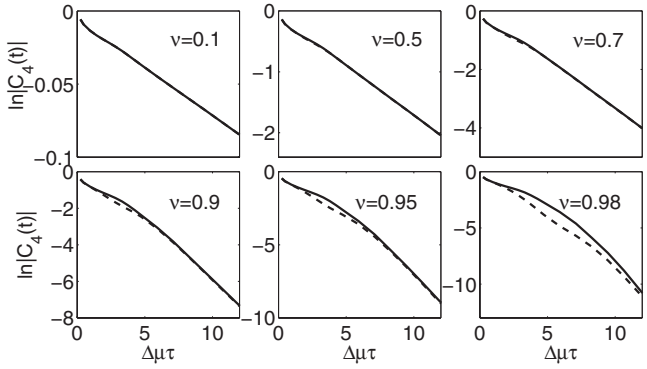

FIG. 15. Testing the Coulomb gas picture for out-of-equilibrium situations. Comparison between the exact fourth order correlation function $C_4(t_1,t_2,t_3,t_4)$, Eq. (42) (full), and the pairwise approximation $\tilde{C}_4(t_1,t_2,t_3,t_4)$, Eq. (43) (dashed). $\tau = t_{i+1} - t_i$ is the distance between spin-flip events. All other parameters are the same as in Fig. 5.

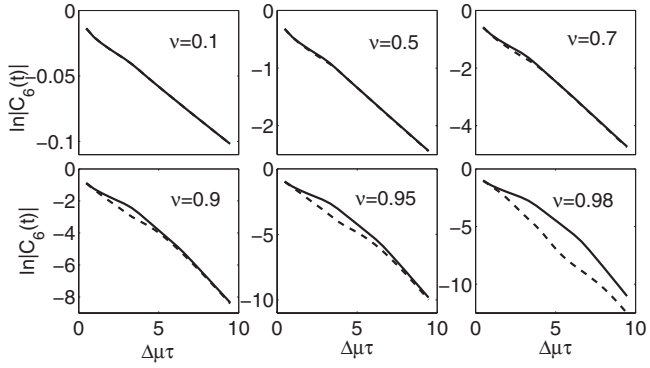

FIG. 16. Testing the Coulomb gas picture for out-of-equilibrium situations. Comparison between the exact expression sixth order correlation function $C_6(t_1,t_2,t_3,t_4,t_5,t_6)$, Eq. (42) (full), and the pairwise approximation $\tilde{C}_6(t_1,t_2,t_3,t_4,t_5,t_6)$, Eq. (43) (dashed). $\tau = t_{i+1} - t_i$ is the distance between spin-flip events. All other parameters are the same as in Fig. 5.

time scales for *arbitrary strong coupling to the leads*.

While previous works have studied the nonequilibrium dynamics in the long time limit,[11,36,39] we have provided information in the intermediate-time domain, where exact analytical results are not available. In the nonadiabatic limit for strong system-lead coupling, we have discovered a nonequilibrium regime with a Marcus-like spin relaxation rate that, to the best of our knowledge, has not been discussed before. Here, while the nonequilibrium dynamics is qualitatively similar to the equilibrium dynamics at a finite temperature, the analogy is not complete. In particular, a simple linear mapping between temperature and bias voltage does not exist, in contrast to the electrically damped harmonic oscillator model.[66,67] The Marcus-like relaxation rate exhibits highly nonlinear current-voltage (I-V) characteristics: The current is practically suppressed at small bias voltage and is strongly enhanced at intermediate bias (of the order of the energy difference between spin levels B), while for large bias, linear I-V behavior emerges.

In the long time limit, a nonequilibrium situation generates complex scattering phase shifts which are reflected in the dynamics through different effects: (i) onset of an exponential decay for the spin polarization, (ii) appearance of a power-law term in the relaxation dynamics, with a complex exponent, and (iii) the possible existence of an antiorthogonality regime. The effects presented in this paper are not limited to the specific model utilized here but can be rederived for other systems, e.g., the resonant level model of Appendix A, where the polarization of a spin impurity couples to the resonant level occupancy.[11]

Going beyond the nonadiabatic limit, we have studied multiple spin-flip events with the aid of exact numerical calculations. Interestingly, we have found that the Anderson-Yuval-Hamann treatment of the equilibrium Kondo effect[65] can be extended to the out-of-equilibrium regime, but only for weak to intermediate system-bath couplings does the standard pairwise Coulomb gas behavior hold qualitatively for all time scales.[13] Deviations occur precisely in time intervals where the Gaussian decay of the correlation function $C_f(t)$ is prominent.

Several future directions are worthy of investigation. First, we have restricted ourselves in this work to zero temperature. Including the effect of finite temperature is straightforward both analytically and numerically.[57] In particular, the mapping $t \to \tanh(\pi k_B T t)$ (Ref. 41) transforms all analytical expressions to those valid at finite (but low $k_B T < \Delta\mu$) temperatures. Similarly, the numerical approach of Sec. IV A may be generalized to arbitrary temperatures. The simple model studied here can be extended in several important ways, including coupling of the quantum subsystem to vibrational degrees of freedom.

Lastly, we have delineated the precise set of regimes where the standard Anderson-Yuval-Hamann Coulomb gas behavior is quantitatively accurate. This lays the groundwork for future exact numerical studies of the spin dynamics for the models discussed here. In particular, standard influence functional methodology may be directly applied in regimes where pairwise Coulomb gas behavior is exhibited.[13] In regimes where deviations exist, numerically exact Monte Carlo without the pairwise assumption may be performed. Both of these approaches are currently being pursued.

ACKNOWLEDGMENTS

This work was supported by NSF (NIRT)-0210426 (D.S. and D.H.R.) and DMR-0705847 (A.J.M.). The authors acknowledge M. S. Hybertsen and A. Mitra for fruitful discussions.

APPENDIX A: SPIN-RESONANT-LEVEL MODEL

We present here a variant of the model system (2) leading to dynamics analogous to Eqs. (34)–(38). The model was presented in Ref. 11 for the analysis of the generalized fluctuation-dissipation relation for out-of-equilibrium systems. It describes a spin system coupled to a spinless resonant level (creation operator $d^\dagger$), which is itself coupled to two electron baths $n=L,R$,

$$H = H_S + H_B^{(f)} + H_{SB}^{(f)},$$

$$H_S = \frac{B}{2}\sigma_z + \frac{\Delta}{2}\sigma_x,$$

$$H_B^{(f)} = \sum_{k,n} \epsilon_k a_{k,n}^\dagger a_{k,n} + \sum_{k,n} V_{k,n}(a_{k,n}^\dagger d + d^\dagger a_{k,n}),$$

$$H_{SB}^{(f)} = J_z d^\dagger d \frac{(I+\sigma_z)}{2}. \tag{A1}$$

Here, B and Δ are the spin parameters, describing the energy gap and the tunneling splitting, respectively. J_z reflects the strength of system-bath interaction, and $V_{k,n}$ is the coupling element of the resonant level to the nth electronic reservoir. I is the identity operator. The relation of this model to the generic Hamiltonian (2) is revealed by diagonalizing $H_B^{(f)}$ and rewriting Eq. (A1) in terms of the new operators as follows:

$$H_B^{(f)} = \sum_{k,n} \epsilon_k c_{k,n}^\dagger c_{k,n},$$

$$H_{SB}^{(f)} = \frac{J_z}{2}(I+\sigma_z) \sum_{k,n,k',n'} \nu_{k,n}^* \nu_{k',n'} c_{k,n}^\dagger c_{k',n'},$$

$$a_{k,n} = \sum_{k',n'} \eta_{k,n;k',n'} c_{k',n'}, \quad d = \sum_{k,n} \nu_{k,n} c_{k,n}. \tag{A2}$$

with $n,n'=L,R$. The coefficients $\nu_{k,n}$ and $\eta_{k,n,k',m}$ are given by[11]

$$\nu_{k,n} = \frac{V_{k,n}}{\epsilon_k - \sum_{k',m} \frac{V_{k',m}^2}{\epsilon_k - \epsilon_{k'} - i\delta}},$$

$$\eta_{k,n;k',n'} = \delta_{k,k'}\delta_{n,n'} - \frac{V_{k,n}\nu_{k',n'}}{\epsilon_k - \epsilon_k' + i\delta}, \tag{A3}$$

where δ goes asymptotically to zero. Next, we assume that the resonant level-lead coupling is a constant, independent of

momentum. The phase shifts, complex numbers in nonequilibrium situations, then become

$$\delta_L = \arctan \frac{\lambda \sin^2(\theta)}{1 - i\lambda \cos^2(\theta)},$$

$$\delta_R = \arctan \frac{\lambda \cos^2(\theta)}{1 + i\lambda \sin^2(\theta)}. \tag{A4}$$

Here, λ is a dimensionless coupling strength and $\tan(\theta)$ determines the asymmetry with respect to coupling to the L and R sides,

$$\lambda = \frac{2J_z}{\Gamma_L + \Gamma_R}, \quad \theta = \arctan(\sqrt{\Gamma_L/\Gamma_R}), \tag{A5}$$

$\Gamma_n = 2\pi V_n^2 \rho$ is the hybridization of the resonant level with the nth reservoir and ρ is the reservoir [Eq. (A1)] density of states. When the system is symmetric, $\Gamma_L = \Gamma_R$, $\theta = \pi/4$, we obtain the following relations:

$$\delta_{eq} = \delta_L + \delta_R = \arctan(\lambda),$$

$$|\delta_L'' - \delta_R''| = \frac{1}{2} \ln(1 + \lambda^2),$$

$$\delta_L^2 + \delta_R^2 = \frac{1}{2}\left[\arctan^2 \lambda - \frac{1}{4} \ln^2(1 + \lambda^2) \right],$$

$$2\delta_L \delta_R = \frac{1}{2}\left[\arctan^2 \lambda + \frac{1}{4} \ln^2(1 + \lambda^2) \right]. \tag{A6}$$

At weak coupling, the correlation function can be derived using the cumulant expansion, as done through Eqs. (21)–(23),

$$\Phi_f(t) = \frac{\lambda^2}{\pi^2} \ln(1 + iDt) + iE_s t + \frac{\lambda^2}{2\pi^2} \Delta\mu t \left[\mathrm{Si}(\Delta\mu t) - \frac{1 - \cos(\Delta\mu t)}{\Delta\mu t} \right] - \frac{\lambda^2}{2\pi^2} [\gamma_e + \ln(\Delta\mu t) - \mathrm{Ci}(\Delta\mu t)], \tag{A7}$$

with $E_s = D\lambda/\pi$. By following the derivation which leads to Eqs. (19), (20), (26), and (27), for the present case, we obtain the spin-resonant-level correlation function at strong coupling,

$$C_f(t) \sim \begin{cases} (Dt)^{-\beta}, & \Delta\mu t \ll 1 \\ (Dt)^{-\beta} e^{-\kappa \Delta\mu^2 t^2}, & \Delta\mu t \sim 1 - 10 \\ (Dt)^{-\beta} (\Delta\mu t)^{\gamma} e^{-\Gamma \Delta\mu t}, & \Delta\mu t \gg 1, \end{cases} \tag{A8}$$

with the coefficients

$$\beta = \arctan^2(\lambda)/\pi^2,$$

$$\Gamma = \frac{1}{4\pi} \ln(1 + \lambda^2),$$

$$\kappa = \frac{\arctan^2(\lambda)}{8\pi^2},$$

$$\gamma = \frac{1}{2\pi^2}\left[\arctan^2 \lambda + \frac{1}{4} \ln^2(1 + \lambda^2) \right]. \tag{A9}$$

We note that the orthogonality-antiorthogonality transition takes place when the exponential $(\delta_L^2 + \delta_R^2)$ changes sign at $\frac{1}{2} \ln(1 + \lambda^2) = \arctan(\lambda)$.

APPENDIX B: DERIVATION OF THE CLASSICAL MARCUS RATE IN THE SPIN-BOSON MODEL

In this appendix, we derive the classical Marcus behavior of a two-level system coupled to an oscillator bath and compare the result to the nonequilibrium Marcus-like behavior found in the main text. The classical Marcus result[45] emerges in the high temperature limit of the asymmetric spin-boson model in the nonadiabatic regime.[1] The Hamiltonian is given by

$$H = H_S + H_B^{(b)} + H_{SB}^{(b)}, \tag{B1}$$

where the spin system H_S includes a two-level system (TLS) with a bare tunneling amplitude Δ and a level splitting B. The reservoir $H_B^{(b)}$ includes a set of independent harmonic oscillators, and the system-bath interaction $H_{SB}^{(b)}$ is bilinear in the reservoir coordinates and the spin polarization,

$$H_S = \frac{B}{2}\sigma_z + \frac{\Delta}{2}\sigma_x,$$

$$H_B^{(b)} = \sum_j \omega_j b_j^\dagger b_j,$$

$$H_{SB}^{(b)} = \sum_j \frac{\lambda_j}{2}(b_j^\dagger + b_j)\sigma_z. \tag{B2}$$

Here, $b_j^\dagger, b_j$ are bosonic creation and annihilation operators, respectively. In the nonadiabatic regime, the excitation rate can be calculated within Fermi's golden rule as[44]

$$\Gamma_b^{\pm} = \left(\frac{\Delta}{2}\right)^2 \int_{-\infty}^{\infty} dt e^{\pm iBt} C_b(t), \quad C_b(t) = e^{-\Phi_b(t)},$$

$$\Phi_b(t) = \sum_j \frac{\lambda_j^2}{\omega_j^2}[(1 + 2n_j) - (1 + n_j)e^{-i\omega_j t} - n_j e^{i\omega_j t}] = \int_0^{\infty} \frac{d\omega}{\pi} \frac{J(\omega)}{\omega^2}\left[1 - e^{-i\omega t} + 4n(\omega) \sin^2 \frac{\omega t}{2} \right], \tag{B3}$$

with spectral function $J(\omega) = \pi \Sigma_j \lambda_j^2 \delta(\omega - \omega_j)$. Here, $n(\omega) = [e^{\omega/k_B T} - 1]^{-1}$ is the Bose-Einstein distribution function with T as the temperature of the bosonic reservoir and k_B the Boltzmann constant. The case relevant to the present paper is the Ohmic spectral density: a continuum of bosons with $J(\omega) = 2\pi\alpha\omega$ at low frequencies and $J(\omega) \to 0$ for ω greater than a cutoff scale ω_c. A conventional choice is

$$J(\omega) = 2\pi\alpha\omega e^{-\omega/\omega_c}, \tag{B4}$$

but most of the results do not depend on this choice. It is useful to decompose Φ_b into two contributions,

$$\Phi_b(t) = \Phi_1(\omega_c t) + \Phi_2(\omega_c t; Tt). \tag{B5}$$

Here,

$$\Phi_1 = \int_0^\infty \frac{d\omega}{\pi}\frac{J(\omega)}{\omega^2}(1 - e^{-i\omega t}),$$

$$\Phi_2 = 4\int_0^\infty \frac{d\omega}{\pi}\frac{J(\omega)}{\omega^2}\frac{\sin^2\frac{\omega t}{2}}{e^{\omega/k_BT} - 1}. \tag{B6}$$

The first term gives the bosonic analog of the zero temperature power-law dependence $\ln(1+iDt)$ found in the main text,

$$\Phi_1(\omega_c t \ll 1) \sim i\lambda t, \quad \lambda \equiv \sum_j \frac{\lambda_j^2}{\omega_j} = 2\alpha\omega_c,$$

$$\Phi_1(\omega_c t \gg 1) \sim 2\alpha \ln(i\omega_c t), \tag{B7}$$

where λ is the solvent reorganization energy. The second term gives the analog of the exponential and/or Gaussian behavior. For $k_BT > \omega_c$, the canonical Marcus result is obtained. In this limit, one approximates $e^{\omega/k_BT} - 1 \to \frac{\omega}{k_BT}$ leading to

$$\Phi_2^{Marcus} = 4k_BT\int_0^\infty \frac{d\omega}{\pi}\frac{J(\omega)}{\omega}\frac{\sin^2\frac{\omega t}{2}}{\omega^2}. \tag{B8}$$

At $\omega_c t \ll 1$, we approximate $\sin^2\frac{\omega t}{2} \sim \omega^2 t^2/4$ and obtain

$$\Phi_2^{Marcus}(\omega_c t \ll 1) = k_BT\lambda t^2. \tag{B9}$$

For $\omega_c t \gg 1$, we may set $J(\omega) = 2\pi\alpha\omega$ and get a linear behavior,

$$\Phi_2^{Marcus}(\omega_c t \gg 1) = 2\pi\alpha k_BT t. \tag{B10}$$

The crossover scale is $t^* = 1/\omega_c$, with the value $\Phi_2^{Marcus}(t^*) \approx 2\alpha k_BT/\omega_c$. Thus, for any α, at large enough k_BT/ω_c, Φ_2 becomes large enough that a Gaussian relaxation results.

The analogy between the high-temperature Marcus behavior and the results we have found in the nonequilibrium fermionic model is not complete, since in the latter case we typically assume that the electron bands are wide relative to the potential bias. We therefore consider next the analogous equilibrium limit of $k_BT < \omega_c$. In this case, the short time limit $[\sin(\omega t/2) \to \omega t/2]$ of Eq. (B6) obeys

$$\Phi_2^T(\omega_c t \ll 1) = 2\alpha t^2\int_0^\infty d\omega\frac{\omega e^{-\omega/\omega_c}}{e^{\omega/k_BT} - 1} \sim \frac{\alpha t^2 k_B^2 T^2 \pi^2}{3}, \tag{B11}$$

while the long time limit reduces to Eq. (B10). We thus obtain a short-time t^2 and a long-time t-linear behavior. The crossover occurs at $t^* \sim 1/k_BT$ and $\Phi_2^T(t^*) = \pi^2\alpha/3 \sim 3\alpha$. Thus, for α much smaller than 1, the relaxation integrals are dominated by the long-time region where $\Phi \sim t$, leading to an exponential relaxation. For $\alpha > 0.5$ however, the power-law prefactor ensures that the integral is dominated by short times, of order ω_c^{-1}, so that the frequency dependence is significant only on the scale of the cutoff scale ω_c.

We compare next this behavior to the nonequilibrium Marcus-like behavior found in the main text. The mathematical essence of the nonequilibrium result is that the time decay function behaves as $\Phi_f \sim \kappa(\Delta\mu t)^2$ at short times and as $\Phi_f \sim \Gamma\Delta\mu t$ at long times; the crossover between these two regimes occurs at $t^* \sim \Gamma/\kappa\Delta\mu$ and the value at t^* is $\Phi_f(t^*) \sim \Gamma^2/\kappa$. In the weak coupling limit $\Gamma \sim \kappa$, $t^* \sim 1/\Delta\mu$ and $\Phi_f(t^*) \sim \Gamma^2/\kappa \sim \nu^2 \ll 1$, so the t^2 behavior is not important for the relaxation rates. However, in the strong coupling limit $\Gamma/\kappa \gg 1$, $t^* \gg 1/\Delta\mu$ and $\Phi_f(t^*) \gg 1$, so that by the time t reaches t^* the evolution function has become negligibly small. In this circumstance, the t^2 behavior controls the relaxation (for all relevant energy differences), leading to the Gaussian behavior discussed in the text. In the nonequilibrium case, the key parameter is therefore Γ^2/κ, and as this becomes larger than unity, Gaussian behavior results. In contrast, in the classical (high temperature) Marcus limit, the role of Γ^2/κ is replaced by $2\alpha k_BT/\omega_c$, while for $k_BT < \omega_c$, the role is played by α. If this is small, one has exponential relaxation, while if this is larger than 1/2, the kinematics is different and the frequency dependence is controlled by the bandwidth scale ω_c. Thus, the nonequilibrium Marcus-like rate discussed here is really another phenomenon.

We proceed and calculate the classical Marcus rate in the high temperature limit. We substitute Eq. (B9) and the short time limit of Eq. (B7) into Eq. (B3), perform the Fourier transform, and recover the Marcus relation for the nonadiabatic rate,

$$\Gamma_b^{\pm} = \left(\frac{\Delta}{2}\right)^2\sqrt{\frac{\pi}{\lambda k_BT}}e^{-(\mp B + \lambda)^2/(4\lambda k_BT)}. \tag{B12}$$

The temperature dependence of the rate constant shows an activated regime for $|\lambda \pm B| \neq 0$, while in the absence of the barrier, $-B = \lambda$, the rate *decreases* with T. The excitation rate Γ_b^- and the emission rate Γ_b^+ are related to one another through an activation factor as

$$\Gamma_b^-/\Gamma_b^+ = e^{-B/k_BT}. \tag{B13}$$

For completeness, we include here other results of the spin-boson model in the nonadiabatic limit: The golden rule rate to lowest order in k_BT/ω_c and B/ω_c yields ($B > 0$) (Ref. 1)

$$\Gamma_b^- = \frac{\Delta^2}{4\omega_c}\left(\frac{\omega_c}{2\pi k_BT}\right)^{1-2\alpha}\frac{|\tilde{\Gamma}(\alpha - iB/2\pi k_BT)|^2}{\tilde{\Gamma}(2\alpha)}e^{-B/2k_BT}. \tag{B14}$$

Here, $\tilde{\Gamma}(x)$ is the complete gamma function. For weak damping, $\alpha \ll 1$, this expression reduces to

$$\Gamma_b^- = \left(\frac{2\pi k_B T}{\Delta_{eff}}\right)^{2\alpha} \frac{\pi\alpha\Delta_{eff}^2}{[(2\alpha\pi k_B T)^2 + B^2]} \frac{B}{e^{B/k_B T} - 1}, \quad \text{(B15)}$$

where Δ_{eff} is an effective tunneling element ($\alpha < 1$),

$$\Delta_{eff} = \Delta[\tilde{\Gamma}(1-2\alpha)\cos(\pi\alpha)]^{1/2(1-\alpha)}(\Delta/\omega_c)^{\alpha/(1-\alpha)}. \quad \text{(B16)}$$

At zero temperature, we can calculate the rate exactly for an arbitrary cutoff frequency ($B > 0$),

$$\Gamma_b^+(T=0) = \frac{\pi\Delta^2}{2\tilde{\Gamma}(2\alpha)\omega_c}\left(\frac{B}{\omega_c}\right)^{2\alpha-1} e^{-B/\omega_c},$$

$$\Gamma_b^-(T=0) = 0. \quad \text{(B17)}$$

As expected, at $T=0$, there are transitions only from the upper level to the lower state.

APPENDIX C: BOSONIZATION OF THE NONEQUILIBRIUM FERMI EDGE HAMILTONIAN

We briefly present here some of the relations between bosonic and fermionic operators and transform our fermionic system-bath Hamiltonian into its bosonic analog via bosonization[26] and discuss the issues involved in bosonizing the nonequilibrium version of the model. For simplicity, instead of the spin-boson Hamiltonian [Eqs. (1) and (2)], we discuss here the x-ray edge Hamiltonian (12), describing the interaction of a localized core hole with two (possibly out of equilibrium) metal leads,

$$H = \sum_{k,n=L,R} \epsilon_k a_{k,n}^\dagger a_{k,n} + \sum_{k,k',n=L,R} V_{n,n} a_{k,n}^\dagger a_{k',n} d^\dagger d + \sum_{k,k'} [V_{L,R} a_{k,L}^\dagger a_{k',R} + V_{R,L} a_{k,R}^\dagger a_{k',L}] d^\dagger d. \quad \text{(C1)}$$

The first term includes two isolated Fermi baths. The second and third terms describe intrabath processes (diagonal coupling) and interbath interactions, respectively. d ($d^\dagger$) are annihilation (creation) operators of the core hole. We consider bands of width D_0 and a constant density of states ρ.

To solve the equilibrium problem, one proceeds as follows. First, one defines new fermion operators ($V_{L,R} = V_{R,L}$)

$$\alpha_{k,+} = \cos\frac{\theta}{2} a_{k,R} + \sin\frac{\theta}{2} a_{k,L}, \quad \text{(C2)}$$

$$\alpha_{k,-} = -\sin\frac{\theta}{2} a_{k,R} + \cos\frac{\theta}{2} a_{k,L}, \quad \text{(C3)}$$

with

$$\tan\theta = \frac{2V_{L,R}}{V_{R,R} - V_{L,L}} \quad \text{(C4)}$$

in terms of which Eq. (C1) becomes

$$H = \sum_{k,n=+,-} \epsilon_k \alpha_{k,n}^\dagger \alpha_{k,n} + \sum_{k,k',n=+,-} V_n \alpha_{k,n}^\dagger \alpha_{k',n} d^\dagger d, \quad \text{(C5)}$$

with $V_\pm = \frac{V_{LL}+V_{RR}}{2} \pm \sqrt{\frac{(V_{R,R}-V_{L,L})^2}{4} + V_{L,R}^2}$. Crucially, in equilibrium, the new fermion variables obey the usual Fermi statistics,

$$\langle \alpha_{k,n}^\dagger \alpha_{k',n'} \rangle = \delta_{k,k'} \delta_{n,n'} f(\epsilon_k / k_B T), \quad \text{(C6)}$$

with $f(\epsilon_k/k_B T)$ as the Fermi-Dirac distribution function. For this reason, each channel can be bosonized, leading to the standard result of Schotte and Schotte for the Fermi edge singularity problem.[25] In a nonequilibrium situation, while the change of basis can be made, the different distribution functions for the left and right leads mean that Eq. (C6) does not hold, preventing bosonization in the transformed basis. One may attempt to proceed by defining the density operator

$$\rho_n(q) = \sum_k a_{k+q,n}^\dagger a_{k,n} \quad (n = L,R), \quad \text{(C7)}$$

which creates particle-hole excitations in the n lead with momentum q. We use it and define bosonic creator and annihilator operators that obey the bosonic commutation relation

$$b_{q,n}^\dagger = \sqrt{\frac{2\pi}{Lq}} \rho_n(q) \quad (q > 0),$$

$$b_{q,n} = \sqrt{\frac{2\pi}{Lq}} \rho_n(-q) \quad (q > 0). \quad \text{(C8)}$$

The distance L is related to the density of states through $\rho = L/2\pi v_F$, with v_F as the velocity at the Fermi energy, taken to be the same for both reservoirs. The fermion field operators,

$$\Psi_n = \frac{1}{\sqrt{L}} \sum_k a_{k,n}, \quad \Psi_n^\dagger = \frac{1}{\sqrt{L}} \sum_k a_{k,n}^\dagger, \quad \text{(C9)}$$

can be expressed in terms of the boson operators as[26]

$$\Psi_n = \lim_{\alpha\to 0} \frac{F_n}{\sqrt{2\pi\alpha}} \exp\left[\sum_q \sqrt{\frac{2\pi}{Lq}} e^{-\alpha q/2} (b_{q,n} - b_{q,n}^\dagger)\right]. \quad \text{(C10)}$$

Here, F_n ($F_n^\dagger$) are the Klein factors that lower (raise) the total fermion number in the n reservoir by 1. The chemical potential difference is therefore concealed inside these factors. α is an arbitrary cutoff that regularizes the theory and mimics a finite bandwidth. Using these expressions, the fermionic Hamiltonian (C1) translates into a bosonic expression as follows:

$$H = H_B + (\Delta_a + \Delta_b) d^\dagger d. \quad \text{(C11)}$$

H includes the isolated reservoir term

$$H_B = \sum_{q,n} v_F q b_{q,n}^\dagger b_{q,n} \quad \text{(C12)}$$

and diagonal (Δ_a) and nondiagonal (Δ_b) contributions

$$\Delta_a = \sum_{q,n} V_{n,n} \sqrt{\frac{qL}{2\pi}} (b^\dagger_{q,n} + b_{q,n}),$$

$$\Delta_b = (\tilde{V}_{L,R} U_L U_R^\dagger + \tilde{V}_{R,L} U_R U_L^\dagger). \tag{C13}$$

Here,

$$U_n = F_n \exp\left(- \sum_q \lambda_q (b^\dagger_{q,n} - b_{q,n}) \right) \quad (n = L,R),$$

$$\lambda_q \equiv \sqrt{\frac{2\pi}{Lq}} e^{-\alpha q/2}. \tag{C14}$$

All the prefactors are absorbed into the coefficient $\tilde{V}_{L,R} = \frac{L}{2\pi\alpha} V_{L,R}$. Equation (C11)–(C13) reveal that for a nonequilibrium system, bosonization yields a *nonlinear* Hamiltonian with a highly nontrivial form. Compared with the solution in the fermionic picture (Appendix D), bosonizing the Hamiltonian does not simplify the calculation, as it does in equilibrium. It should be noted, however, that the use of Eqs. (C11), (C13), and (C14) yields second cumulant expressions identical to those derived in Appendix D.

APPENDIX D: DERIVATION OF THE SECOND CUMULANT EXPRESSION

We derive here the details of the weak coupling correlation function Eq. (22). The second cumulant is given by

$$K_2(t) = -\frac{1}{2} \int_0^t dt_1 \int_0^t dt_2 \langle T F(t_1) F(t_2) \rangle_c, \tag{D1}$$

where $F = \Sigma_{k,k',n,n'} V_{n,n'} a^\dagger_{k,n} a_{k',n'}$, $\langle \cdots \rangle_c$ denotes a cumulant average, and T denotes time ordering. For simplicity, we disregard diagonal interactions, $V_{L,L} = V_{R,R} = 0$. The integrand is calculated using Wick's theorem[44] to yield

$$C_2(\tau) \equiv \langle T F(\tau) F(0) \rangle_c = (\rho V_{L,R})^2 \left[\int_{-D_0}^{\mu_L} d\epsilon_1 \int_{\mu_R}^{D_0} d\epsilon_2 e^{i(\epsilon_1 - \epsilon_2)\tau} + \int_{-D_0}^{\mu_R} d\epsilon_2 \int_{\mu_L}^{D_0} d\epsilon_1 e^{-i(\epsilon_1 - \epsilon_2)\tau} \right]. \tag{D2}$$

Here, $2D_0$ is the bandwidth, ρ is the energy independent density of states, and μ_L (μ_R) is the chemical potential at the L (R) lead. This expression assumes zero temperature. Assuming wide bands, $\mu_K < D_0$, the integrals in Eq. (D2) can be trivially performed producing

$$C_2(\tau) = -2(\rho V_{L,R})^2 \left(\frac{1 - e^{-iD_0\tau}}{\tau} \right)^2 \cos(\Delta\mu\tau) \xrightarrow{D_0\tau \gg 1} 2(\rho V_{L,R})^2 \frac{D_0^2}{(1 + iD_0\tau)^2} \cos(\Delta\mu\tau), \tag{D3}$$

with the voltage difference $\Delta\mu = \mu_L - \mu_R$. In equilibrium, the correlation function is therefore given by

$$C_2^{eq}(t) = 2 \frac{(\rho V_{L,R})^2 D_0^2}{(1 + iD_0 t)^2}. \tag{D4}$$

We substitute this expression into Eq. (D1) and obtain the second cumulant approximation for equilibrium situations,

$$K_2^{eq}(t) = -(\rho V_{L,R})^2 \ln(1 + D_0^2 t^2). \tag{D5}$$

This is the standard result for Tomonaga's model.[25] In nonequilibrium situations, $\Delta\mu \neq 0$, the correlation function includes an oscillatory function, Eq. (D3), which can be decomposed into its equilibrium and nonequilibrium contributions as follows:

$$C_2^{neq}(t) = C_2^{eq}(t) + C_2^{\Delta\mu}(t),$$

$$C_2^{\Delta\mu}(t) = \frac{2(\rho V_{L,R})^2 D_0^2}{(1 + iD_0 t)^2} [\cos(\Delta\mu t) - 1]. \tag{D6}$$

The equilibrium term yields Eq. (D5). We proceed with the nonequilibrium part. For $\Delta\mu \ll D_0$, $D_0 t > 1$,

$$\begin{aligned} K_2^{\Delta\mu}(t) &\sim (\rho V_{L,R})^2 \int_0^t dt_1 \int_0^t dt_2 \frac{\cos(\Delta\mu(t_1 - t_2) - 1)}{(t_1 - t_2)^2} \\ &= -(\rho V_{L,R})^2 \Delta\mu \int_0^t dt_1 \int_0^t dt_2 \frac{\sin(\Delta\mu(t_1 - t_2))}{t_1 - t_2} \\ &\quad + (\rho V_{L,R})^2 \int_0^t dt_1 \int_0^t dt_2 \frac{d}{dt_2} \left[\frac{\cos(\Delta\mu(t_1 - t_2)) - 1}{t_1 - t_2} \right]. \end{aligned} \tag{D7}$$

Exact integration leads to

$$\begin{aligned} K_2^{\Delta\mu}(t) &= -2(\rho V_{L,R})^2 \{ \Delta\mu t \, \mathrm{Si}(\Delta\mu t) - [1 - \cos(\Delta\mu t)] \} \\ &\quad + 2(\rho V_{L,R})^2 [\gamma_e + \ln(\Delta\mu t) - \mathrm{Ci}(\Delta\mu t)]. \end{aligned} \tag{D8}$$

The sine and cosine integrals are defined as $\mathrm{Si}(x) = \int_0^x \frac{\sin(t)}{t} dt$, $\mathrm{Ci}(x) = \gamma_e + \ln(x) + \int_0^x \frac{\cos(t) - 1}{t} dt$, and $\gamma_e = 0.5772$ is the Euler-Mascheroni constant. In deriving Eq. (D8), we have used the following identities: $\int \mathrm{Si}(x) dx = \cos(x) + x\mathrm{Si}(x)$ and $\int_0^x \frac{\sin[(t-\alpha)\beta]}{t-\alpha} dt = \mathrm{Si}[(x-\alpha)\beta] - \mathrm{Si}(\alpha\beta)$. The sum of Eqs. (D5) and (D8) is our expression for the second cumulant [Eq. (22)] with $\nu = \pi\rho V_{L,R}$. After exponentiating, the first term provides an exponential relaxation at long times, while the second term yields a power-law contribution.

APPENDIX E: APPROXIMATE ANALYTICAL EVALUATION OF RATE CONSTANTS

In this appendix, we present a derivation of the rate constants in the important limiting cases. We begin from the basic expression [Eq. (33)]

$$\Gamma_f^+(\omega) = \mathrm{Re} \int_0^\infty \frac{dt}{(iDt)^{\beta_{eff}(t)}} e^{i\omega t - A(t)}. \tag{E1}$$

Here, D is an energy scale of the order of the bandwidth, and β_{eff} is an effective exponent which changes from the equi-

librium power β to the nonequilibrium power β_{neq}. The results of Sec. IV imply that

$$A(t) = g\phi\left(\frac{t}{t^*}\right), \tag{E2}$$

with ϕ defined such that $\phi(x\to 0)\to x^2$ and $\phi(x\to\infty)\to x$. This implies that the coupling constant g and characteristic time t^* are

$$g = \frac{\Gamma^2}{\kappa}, \tag{E3}$$

$$t^* = \frac{\Gamma}{\kappa\Delta\mu}. \tag{E4}$$

In the weak coupling limit ($\nu \ll 1$), $\Gamma \sim \kappa \sim \nu^2$ so $g \ll 1$ and $t^* \sim (\Delta\mu)^{-1}$, while in the strong coupling limit ($\nu \sim 1$), $\Gamma \to \infty$ while κ saturates so $g \gg 1$ and $t^* \gg (\Delta\mu)^{-1}$. We define a dimensionless time coordinate $u = t/t^*$ and frequency $\omega^* = \omega t^*$ in terms of which the dimensionless relaxation rate $D\Gamma_f^+$ becomes

$$D\Gamma_f^+(\omega) = \mathrm{Re}\int_0^\infty \frac{du}{(iu)^{\beta_{eff}(u)}}(Dt^*)^{1-\beta_{eff}(u)}e^{i\omega^* u - g\phi(u)}. \tag{E5}$$

The analysis of the integral in Eq. (E5) requires some care because the scales which dominate the integral may not be the scales which dominate the real part of the integral. To isolate the contributions to the real part, we deform to contour into the complex plane. Writing $u = x + iy$, we deform the integration contour into two parts, one running along the imaginary axis ($x=0$) to the point $y=y^*$ at which $i\omega^* - g\partial\phi/\partial y = 0$ and another running parallel to the real axis along the contour $u = x + iy^*$. Thus, we have

$$D\Gamma_f^+(\omega) = I_1 + I_2, \tag{E6}$$

with

$$I_1 = \mathrm{Im}\int_0^{y^*} dy \frac{(Dt^*)^{1-\beta_{eff}(y)}}{(-y)^{\beta_{eff}(y)}}e^{-\omega^* y - g\phi(iy)}, \tag{E7}$$

$$I_2 = e^{-|\omega^* y^*|}\,\mathrm{Re}\int_0^\infty dx \frac{(Dt^*)^{1-\beta_{eff}(x+iy^*)}}{(ix-y^*)^{\beta_{eff}(x+iy^*)}}e^{i\omega^* x - g\phi(x+iy^*)}. \tag{E8}$$

Here, Re refers to the real part of the integral and Im to the imaginary part. We analyze these equations first in weak coupling $g<1$. Let us begin with I_1. Inspection of the second cumulant formula shows that $y^*<0$ if $\omega<0$. In this case, the integral does not have any imaginary part so for $\omega<0$, $I_1 = 0$. Next consider small positive ω, where we may approximate $\phi(y)=y^2$ implying

$$y^* = \frac{\omega^*}{2g} = \frac{\omega}{2\Gamma\Delta\mu}. \tag{E9}$$

Thus, for $\omega<\Gamma\Delta\mu$, we may use the equilibrium exponent and approximate $\phi=y^2$ obtaining

$$I_1 = \Theta(\omega)\sin(\pi\beta)(Dt^*)^{1-\beta}\int_0^{\omega/2\Gamma\Delta\mu}\frac{dy}{y^\beta}e^{-\omega^* y + gy^2}. \tag{E10}$$

At the endpoint $\frac{\omega^*}{2g}$, the argument of the exponential is minimized; the minimum value is $-\frac{(\omega^*)^2}{4g} = -\frac{\omega^2}{4\kappa\Delta\mu^2}$. Substituting the maximum value $\omega = \Gamma\Delta\mu$ and noting that in weak coupling $\Gamma \sim \kappa \ll 1$, we see that the argument of the exponential is negligible over the entire range $\omega<\Gamma\Delta\mu$, and we get

$$I_1 = \Theta(\omega)\frac{\sin(\pi\beta)}{1-\beta}\left(\frac{D\omega}{2\Gamma\Delta\mu^2}\right)^{1-\beta}. \tag{E11}$$

For $\omega>\Gamma\Delta\mu$, $y^*>1$, and we must consider the form of ϕ for large imaginary argument. Inspection of the second cumulant formula shows that

$$\phi(iy) \sim \cosh(y) \sim e^y, \tag{E12}$$

implying $y^* \sim \ln(\omega^*/g)$. In this case, the value of the argument of the exponential at the upper limit of integration is $-\omega^*\ln(\omega^*/g) \sim -(\omega/\Delta\mu)\ln[\omega/(\Gamma\Delta\mu)]$. Thus, for $\omega \gtrsim \frac{\Delta\mu}{\ln(1/\Gamma)}$, the upper limit of the integral may be set to infinity, and for $\omega \gtrsim \Delta\mu$, the integral is dominated by $y<1$ yielding

$$D\Gamma_f^+(\omega) = \mathrm{Im}(-1)^{-\beta}(Dt^*)^{1-\beta}\int_0^\infty \frac{dz}{z^\beta}e^{-\omega^* z} \tag{E13a}$$

$$= \sin(\pi\beta)\left(\frac{D}{\omega}\right)^{1-\beta}\tilde{\Gamma}(1-\beta). \tag{E13b}$$

Here, $\tilde{\Gamma}(x)$ is the complete gamma function. Equation (E13b) is simply the usual equilibrium result. Therefore, in weak coupling, I_1 is given by Eq. (E11) for $\omega \lesssim \Delta\mu/\ln\Gamma^{-1}$ and by Eq. (E13b) for $\omega \gtrsim \Delta\mu$, with a rather broad crossover regime.

We next turn to I_2 which is nonzero for both signs of ω. The frequency regimes are as for I_1. For $\omega<\Delta\mu/\ln\Gamma^{-1}$, the integral is dominated by large x, where $\phi=x$ and the prefactor $e^{-|\omega^* y^*|}$ is negligible, so that we find

$$I_2 \approx (D)^{1-\beta_{neq}}\tilde{\Gamma}(1-\beta_{neq})\mathrm{Re}\left[\frac{e^{-i\pi\beta_{neq}/2}}{(i\omega-\Gamma\Delta\mu)^{1-\beta_{neq}}}\right]. \tag{E14}$$

Note that we have replaced β by the long-time nonequilibrium value β_{neq}. In the weak coupling limit, $\beta_{neq} \sim \nu^4 \ll 1$. Setting $\beta_{neq}\to 0$ yields a Lorentzian behavior

$$I_2 = \frac{D\Gamma\Delta\mu}{\omega^2 + \Gamma^2\Delta\mu^2}. \tag{E15}$$

Note that for $\omega>0$ I_2 only becomes smaller than I_1 for $\omega \sim \Gamma\Delta\mu/\sin\beta\pi \sim \Delta\mu$. As ω becomes of the order of $\Delta\mu/\ln\Gamma^{-1}$, the prefactor begins to be important and I_2 decays proportional to $e^{-(\omega/\Delta\mu)\ln(\omega/\Delta\mu)}$ as found by Mitra *et al.*[10]

To summarize, for weak coupling, we find a rate which for small frequencies, $\omega<\Delta\mu/\ln\Gamma^{-1}$, is approximately Lorentzian, with decay constant $\Gamma\Delta\mu$. On the emission (positive frequency) side, the Lorentzian decay is overcome by the contribution of I_1 and eventually crosses over the

equilibrium rate, Eq. (E13b), while on the absorption (negative frequency) side, the rate crosses over to into the $e^{-(\omega/\Delta\mu)\ln(\omega/\Delta\mu)}$ relaxation.

We now take up the strong coupling ($g>1$) limit. For $\omega<\Gamma\Delta\mu$, Eq. (E10) still applies, but now at the endpoint of the integration region, the argument of the exponential can be large. For $\omega^*<\sqrt{g}$ (i.e., $\omega<\sqrt{\kappa}\Delta\mu$), the variation of the exponent is not important, and we get

$$I_1^{(A)}=\Theta(\omega)\frac{\sin(\pi\beta)}{1-\beta}\left(\frac{D\omega}{2\kappa\Delta\mu^2}\right)^{1-\beta},\quad |\omega|\ll\sqrt{\kappa}\Delta\mu. \tag{E16}$$

In contrast, in the opposite high frequency limit, we can set the upper limit of the integration to infinity and drop the y^2 term. This yields

$$I_1^{(B)}=\Theta(\omega)\sin(\pi\beta)\left(\frac{D}{\omega}\right)^{1-\beta}\tilde{\Gamma}(1-\beta),\quad \omega>\sqrt{\kappa}\Delta\mu, \tag{E17}$$

which is again the equilibrium ($\Delta\mu=0$) result. This continues to apply even for $\omega>\Gamma\Delta\mu$. We next turn to I_2. For $\omega<\Gamma\Delta\mu$, we again approximate $\phi=(x+iy^*)^2$ and find

$$I_2=e^{-(\omega^2/4\kappa\Delta\mu^2)}(Dt^*)^{1-\beta}\,\mathrm{Re}\left[\int_0^\infty\frac{dx}{\left(ix-\frac{\omega}{2\Gamma\Delta\mu}\right)^\beta}e^{-gx^2}\right]. \tag{E18}$$

The important x are of order $\sqrt{g}$, so that for $\omega<\sqrt{\kappa}\Delta\mu$, we may neglect the ω in the denominator and get

$$I_2^{(A)}=\cos\frac{\pi\beta}{2}e^{-(\omega^2/4\kappa\Delta\mu)}\left(\frac{D}{\sqrt{\kappa}\Delta\mu}\right)^{1-\beta}\frac{\tilde{\Gamma}[(1-\beta)/2]}{2},\quad |\omega|<\sqrt{\kappa}\Delta\mu. \tag{E19}$$

In the opposite limit, $|\omega|>\sqrt{\kappa}\Delta\mu$, we neglect x in the denominator and find

$$I_2^{(B)}=e^{-(\omega^2/4\kappa\Delta\mu^2)}\cos(\pi\beta)\frac{D}{2\sqrt{\kappa}\Delta\mu}\left(\frac{2\kappa\Delta\mu^2}{D\omega}\right)^{\beta},\quad |\omega|>\sqrt{\kappa}\Delta\mu. \tag{E20}$$

For the emission rate $\omega>0$, the Marcus rate given by Eq. (E20) goes over to the equilibrium power-law behavior, Eq. (E17), when $I_2^{(B)}$ becomes smaller than $I_1^{(A)}$, which happens for ω slightly larger than $2\sqrt{\kappa}\Delta\mu$.

Finally, if $\omega^*>g$ ($\omega>\Gamma\Delta\mu$), then the approximation $\phi=y^2$ does not apply and the rate goes over the $e^{-\omega\ln\omega}$ form discussed above. However, by this time, the rate is so small that this behavior is not relevant.

*Corresponding author. Present address: Chemical Physics Theory Group, Department of Chemistry, University of Toronto, Ontario, Canada M5S 3H6. dsegal@chem.utoronto.ca

[1] U. Weiss, *Quantum Dissipative Systems* (World Scientific, Singapore, 1993).
[2] J. Kondo, Prog. Theor. Phys. **32**, 37 (1964).
[3] A. C. Hewson, *The Kondo Problem to Heavy Fermions* (Cambridge University Press, Cambridge, England, 1993).
[4] A. M. Kuznetsov and I. Ulstrup, *Electron transfer in Chemistry and Biology* (Wiley, Chichester, UK, 1999).
[5] R. P. Bell, *The Tunnel Effect in Chemistry* (Chapman and Hall, London, 1980).
[6] A. Muller, H. Ratajczak, W. Junge, and E. Diemann, *Electron and Proton Transfer in Chemistry and Biology* (Elsevier, New York, 1992).
[7] A. J. Leggett, S. Chakravarty, A. T. Dorsey, M. P. Fisher, A. Garg, and W. Zwerger, Rev. Mod. Phys. **59**, 1 (1987).
[8] F. Lesage, H. Saleur, and S. Skorik, Phys. Rev. Lett. **76**, 3388 (1996); F. Lesage and H. Saleur, *ibid.* **80**, 4370 (1998).
[9] A. Mitra, I. Aleiner, and A. J. Millis, Phys. Rev. B **69**, 245302 (2004).
[10] A. Mitra, I. Aleiner, and A. J. Millis, Phys. Rev. Lett. **94**, 076404 (2005).
[11] A. Mitra and A. J. Millis, Phys. Rev. B **72**, 121102(R) (2005).
[12] A. Mitra, S. Takei, Y. B. Kim, and A. J. Millis, Phys. Rev. Lett. **97**, 236808 (2006).
[13] A. Mitra and A. J. Millis, Phys. Rev. B **76**, 085342 (2007).
[14] G. Zarand and A. Zawadowski, Phys. Rev. Lett. **72**, 542 (1994).
[15] A. Rosch, J. Paaske, J. Kroha, and P. Wolfle, Phys. Rev. Lett. **90**, 076804 (2003).
[16] J. Paaske, A. Rosch, and P. Wolfle, Phys. Rev. B **69**, 155330 (2004).
[17] J. Paaske, A. Rosch, J. Kroha, and P. Wolfle, Phys. Rev. B **70**, 155301 (2004).
[18] S. Kehrein, Phys. Rev. Lett. **95**, 056602 (2005).
[19] P. Mehta and N. Andrei, Phys. Rev. Lett. **96**, 216802 (2006).
[20] B. Doyon and N. Andrei, Phys. Rev. B **73**, 245326 (2006).
[21] R. M. Potok, I. G. Rau, H. Shtrikman, Y. Oreg, and D. Goldhaber-Gordon, Nature (London) **446**, 167 (2007).
[22] S. De Franceschi, R. Hanson, W. G. van der Wiel, J. M. Elzerman, J. J. Wijpkema, T. Fujisawa, S. Tarucha, and L. P. Kouwenhoven, Phys. Rev. Lett. **89**, 156801 (2002).
[23] *Molecular Nanoelectronics*, edited by M. A. Reed and T. Lee (American Scientific, Stevenson Ranch, CA, 2003).
[24] A. Nitzan and M. A. Ratner, Science **300**, 1384 (2003).
[25] K. D. Schotte and U. Schotte, Phys. Rev. **182**, 479 (1969).
[26] T. Giamarchi, *Quantum Physics in One Dimension* (Oxford University Press, Oxford, 2003).
[27] F. Guinea, V. Hakim, and A. Muramatsu, Phys. Rev. B **32**, 4410 (1985).
[28] A. S. Alexandrov, A. M. Bratkovsky, and R. S. Williams, Phys. Rev. B **67**, 075301 (2003).

[29] A. Komnik and A. O. Gogolin, Phys. Rev. B **69**, 153102 (2004).
[30] M. Galperin, M. A. Ratner, and A. Nitzan, Nano Lett. **5**, 125 (2005).
[31] M. Galperin, M. A. Ratner, and A. Nitzan, J. Phys.: Condens. Matter **19**, 103201 (2007).
[32] P. Nozieres and C. T. De Dominicis, Phys. Rev. **178**, 1097 (1969).
[33] K. Ohtaka and Y. Tanabe, Rev. Mod. Phys. **62**, 929 (1990).
[34] D. A. Abanin and L. S. Levitov, Phys. Rev. Lett. **93**, 126802 (2004).
[35] M. Hentschel, D. Ullmo, and H. U. Baranger, Phys. Rev. B **72**, 035310 (2005).
[36] T. K. Ng, Phys. Rev. B **51**, 2009 (1995); **54**, 5814 (1996).
[37] M. Combescot and B. Roulet, Phys. Rev. B **61**, 7609 (2000).
[38] B. Braunecker, Phys. Rev. B **68**, 153104 (2003).
[39] B. Muzykantskii, N. d'Ambrumenil, and B. Braunecker, Phys. Rev. Lett. **91**, 266602 (2003).
[40] N. d'Ambrumenil and B. Muzykantskii, Phys. Rev. B **71**, 045326 (2005).
[41] B. Braunecker, Phys. Rev. B **73**, 075122 (2006).
[42] D. A. Abanin and L. S. Levitov, Phys. Rev. Lett. **94**, 186803 (2005).
[43] T. Holstein, Ann. Phys. (N.Y.) **8**, 325 (1959); **8**, 343 (1959).
[44] G. D. Mahan, *Many-Particle Physics* (Plenum, New York, 2000).
[45] R. A. Marcus, J. Chem. Phys. **24**, 979 (1956); **43**, 679 (1965); Rev. Mod. Phys. **65**, 599 (1993).
[46] D. Segal, D. R. Reichman, and A. J. Millis (unpublished).
[47] The Hamiltonian (2) could also be defined using a symmetric form for the system-bath interaction $\bar{H}_{SB}^{(f)} = \sigma_z \Sigma_{k,n;k',n'} \frac{V_{k,n;k',n'}}{2} a_{k,n}^{\dagger} a_{k',n'}$. The resulting equilibrium and nonequilibrium phase shifts then relate to Eqs. (5)–(8) by $\bar{\delta}_{\pm} = 2\delta_{\pm}(\alpha_1/2, \alpha_2/2, \nu/2)$ and $\bar{\delta}_{L,R} = 2\delta_{L,R}(\alpha_1/2, \alpha_2/2, \nu/2)$.
[48] N. N. P. Moonen, A. H. Flood, J. M. Fernandez, and J. F. Stoddart, Top. Curr. Chem. **262**, 99 (2005).
[49] W. Liang, M. P. Shores, M. Bockrath, J. R. Long, and H. Park, Nature (London) **417**, 725 (2002).
[50] G. Hackenbroich, B. Rosenow, and H. A. Weidenmuller, Phys. Rev. Lett. **81**, 5896 (1998).
[51] Y. C. Chen, J. Stat. Phys. **47**, 17 (1987).
[52] L. D. Chang and S. Chakravarty, Phys. Rev. B **31**, 154 (1985).
[53] C. Aslangul, N. Pottier, and D. Saint-James, Phys. Lett. **110A**, 249 (1985).
[54] M. Lax, J. Chem. Phys. **20**, 1752 (1952).
[55] R. Kubo and Y. Toyozawa, Prog. Theor. Phys. **13**, 160 (1955).
[56] A. A. Golosov, D. R. Reichman, and E. Rabani, J. Chem. Phys. **118**, 457 (2003).
[57] At finite temperature, the following equality holds: $\mathrm{Tr}[\hat{\rho}\hat{R}] = \det[fR + (1-f)]$, (Refs. 34 and 41) connecting the many-body representation at the left-hand side to a single particle representation at the right-hand side. At the left side, $\hat{R}$ is a many-body operator of interest, $\hat{\rho}$ is the initial density matrix, and the trace is performed over all many-body states. At the right side, f is the (finite temperature) Fermi distribution function, and R represents the matrix elements of $\hat{R}$ taken between the *single particle* states.
[58] K. G. Wilson, Rev. Mod. Phys. **47**, 773 (1975).
[59] L. N. Oliveira and J. W. Wilkins, Phys. Rev. B **24**, 4863 (1981).
[60] M. Yoshida, M. A. Whitaker, and L. N. Oliveira, Phys. Rev. B **41**, 9403 (1990).
[61] P. W. Anderson, Phys. Rev. Lett. **18**, 1049 (1967).
[62] For strong bias ($\Delta\mu \sim D$), the second cumulant (Appendix D) yields at intermediate times $K_2(\Delta\mu t \sim 1) = -(\rho V)^2 D \Delta\mu t^2/2$. For strong coupling, following the discussion in Sec. III B, we find that $\Phi_{neq}(t) \sim \kappa D \Delta\mu t^2$, see Eq. (27). Substituting this result into Eq. (31) yields the "normal" Marcus rate with reorganization energy $\lambda_f = \kappa D$ and driving force $F = \Delta\mu$, in full analogy with the bosonic system.
[63] S. A. Gurvitz, Phys. Rev. B **56**, 15215 (1997).
[64] L.-D. Chang and S. Chakravarty, Phys. Rev. B **31**, 154 (1985).
[65] P. W. Anderson, G. Yuval, and D. R. Hamann, Phys. Rev. B **1**, 4464 (1970).
[66] D. Mozyrsky and I. Martin, Phys. Rev. Lett. **89**, 018301 (2002).
[67] M. B. Hastings, I. Martin, and D. Mozyrsky, Phys. Rev. B **68**, 035101 (2003).